Dust in the Wind: Air Quality and the Drying of the Great Salt Lake

Lena Harris, Eric Edwards, Danae Hernandez-Cortes*

March 24, 2026

Abstract

Air pollution from natural sources is often subject to less regulatory oversight, but can still be caused by human activities. Understanding the role for policy requires quantifying the source's pollution contribution, for which there is currently no standard methodological approach. This paper uses the context of the shrinking Great Salt Lake in Utah to model air quality impacts of the highly erodible and growing area of exposed lakebed described as an "environmental nuclear bomb." Causal estimates of the pollution caused by the lake do not exist, a gap we fill using four common identification strategies in the air pollution literature, and three alternative pollution measurement technologies. We find consistent evidence of meaningful pollution increases attributable to the shrinking lake. Estimates are relatively invariant to measurement technology, but are highly dependent on identification strategy, with marginal annual costs ranging from about $2.6 million to $172 million per 100 km^2 of exposed lakebed. Scaling to the area of total exposed lakebed, annual desiccation-related health cost estimates range from $35 million and $2.3 billion. Given the direct relationship between human water use in the basin and exposed lakebed, these results provide evidence for the cost-effectiveness of policies aimed at reducing consumptive water use.

*Harris: Texas A&M University, lenaharris@tamu.edu, Edwards: UC Davis, ecedwar@ucdavis.edu, Hernandez-Cortes: Arizona State University and NBER, Danae.Hernandez-Cortes@asu.edu. We did not receive outside funding for this project.

1 Introduction

Air pollution from natural sources has typically received less policy attention than direct emissions. Under the U.S. Clean Air Act, the Exceptional Events Rule allows air quality measurements influenced by natural phenomena, including wildfires and high-wind dust events, to be excluded from regulatory determinations, provided the event was not reasonably controllable or preventable (U.S. Environmental Protection Agency, 2016; U.S. Environmental Protection Agency, 2020). This designation essentially grants a "regulatory force majeure," limiting the incentives for proactive policy actions that prevent pollution from natural sources (Williams, 2021).

Until recently, and perhaps due to these types of policy exemptions, less attention has been paid to natural air pollution events in the environmental economics literature. That focus has shifted as evidence has accumulated linking natural resource use and policy decisions to the frequency and severity of these events. Two prominent examples are wildfire smoke (e.g. Burke et al., 2023; Borgschulte, Molitor, and Zou, 2024) and dust storms (Jones and Fleck, 2020; Abman, Edwards, and Hernandez-Cortes, 2025). In the case of wildfires, underinvestment in fuel treatments and constraints on forest management have increased fuel loads and fire intensity, contributing to large smoke-related pollution episodes. Similarly, dust emissions associated with the desiccation of terminal lakes are increasingly understood to be the consequence of upstream water diversions, creating a direct connection between human activity and airborne dust pollution.

Windblown particulate matter from lakebeds exposed due to anthropogenic water diversions has emerged as a key policy challenge. These emissions can affect air quality over large areas and for extended periods, but there is limited causal evidence on their contribution to pollution. Existing studies show that mineral and soil dust can account for a substantial share of particulate matter, often comprising 30–50 percent of PM_{10} during dust events and contributing meaningfully to $PM_{2.5}$ concentrations as well (Querol et al., 2019; Liang et al., 2022; Krasnov et al., 2014).

Owens Lake in California, which disappeared entirely soon after water diversions to the city of Los Angeles began in 1913, became one of the most significant sources of particu-

late air pollution in the United States. In 1997, the U.S. Environmental Protection Agency reported that "air monitoring of the Owens Valley during the past 18 years has measured the highest particulate matter (PM_{10}) pollution in the United States" (U.S. Environmental Protection Agency, 1997). After the region was designated as nonattainment under the Clean Air Act, the lakebed was identified as the dominant source of PM_{10} and the local air regulator pursued enforcement actions against Los Angeles. These actions included a stipulated judgment in 2014 requiring long-term dust mitigation. Since then, Los Angeles has spent over $2.6 billion in aggregate on dust control measures, with annual operating and maintenance costs on the order of $40–45 million, to control emissions across approximately 48.6 square miles of playa (Los Angeles Department of Water and Power, 2025).

In this paper, we examine emissions from another terminal lake, the Great Salt Lake (GSL) in Utah, where water diversions, primarily for agricultural irrigation, have reduced lake levels over the past century (Wurtsbaugh et al., 2017). These declines have accelerated since the late twentieth century, reducing lake surface area by more than half and substantially increasing exposed playa. GSL is an order of magnitude larger than Owens Lake, historically 2,300–3,300 square miles, and its desiccation has been described as an "environmental nuclear bomb" (Flavelle, 2022).

Studies of dried or drying lakebeds in Morocco and Central Asia document increased particulate exposure and associated respiratory and cardiovascular health risks in downwind communities (Jones et al., 2015; Burke et al., 2018). Studies in the western United States show how agricultural water diversions that reduce surface water availability can increase dust emissions and particulate exposure (Jones, Wang, and Fleck, 2025), with disproportionate impacts on nearby and disadvantaged communities (Abman, Edwards, and Hernandez-Cortes, 2025). More broadly, exposure to desert and crustal dust has been linked to increased hospital admissions and mortality (Querol et al., 2019; Aragon and Rud, 2021).

Despite emerging research in other locations, causal estimates of the public health consequences of GSL desiccation do not exist, a gap this paper fills by examining how the increasing area of exposed lakebed has impacted observed particulate levels. We focus on two related research questions. First, how much pollution does exposed lakebed generate? Second, how do commonly used identification strategies perform for a large, diffuse source?

Because terminal lake desiccation is the result of water policy choices, estimates of the effects of pollution and health costs inform policy choices. Policies that reduce water diversions to stabilize lake levels impose real economic costs on agricultural and urban water users. Pollution cost estimates are needed to understand tradeoffs, for instance in performing benefit-cost analyses of regulatory actions.

In addition to informing water policy decisions, this paper contributes to the literature by systematically comparing several commonly used identification strategies from the point-source emissions literature as applied to lakebed emissions. Because natural sources lack a single emission point and are not directly monitored, adapting these approaches to this setting is itself a novel contribution. To evaluate how well existing identification strategies perform in this context, we estimate pollution impacts using four empirical designs: a near–far differences framework, two wind-based approaches that exploit downwind exposure, and a particle transport model based on HYSPLIT. Each method is implemented using EPA monitors, PurpleAir monitors, and satellite-derived pollution measures, which allows us to assess robustness across both identification strategy and data source.

We also examine the role of low-cost PurpleAir monitors alongside regulatory and satellite data. While EPA monitors provide high-quality measurements, their spatial coverage is limited. These limitations are especially constraining for analysis of large, diffuse emission sources like dry lakebeds. PurpleAir sensors offer dense spatial resolution but introduce concerns regarding measurement error and comparability, while satellite-derived measures provide broad coverage at the cost of temporal aggregation and modeling assumptions. Despite their growing use, there is limited evidence on how estimates differ across these data sources when paired with alternative identification strategies. By evaluating these combinations within a single empirical setting, this paper provides guidance for applied research using emerging air quality monitoring data.

Across all four empirical approaches, we find consistent evidence that Great Salt Lake desiccation leads to economically meaningful increases in particulate pollution, though the estimated magnitude varies substantially by identification strategy. The simpler near–far design implies that a 100 km^2 increase in exposed lakebed raises $PM_{2.5}$ concentrations by roughly 0.6–0.7 $\mu g/m^3$ within 30 km of the lake, with detectable effects extending out to

about 100 km. Wind-based approaches that incorporate directional exposure produce larger and more spatially concentrated estimates: both the hours-downwind and angle-downwind models show peak marginal effects above 2 $\mu g/m^3$ per 100 km^2 of additional exposed playa in the most exposed downwind areas, with effects around 1 $\mu g/m^3$ for moderately exposed locations. By contrast, the particle transport model based on HYSPLIT yields smaller implied concentration responses, with back-of-the-envelope conversions suggesting increases on the order of 0.01–0.03 $\mu g/m^3$ for typical exposure levels per 100 km^2. Notably, while effect magnitudes differ across identification strategies, results are comparatively stable across measurement technologies—EPA regulatory monitors, PurpleAir sensors, and satellite-derived pollution fields produce similar gradients and spatial patterns conditional on the modeling approach.

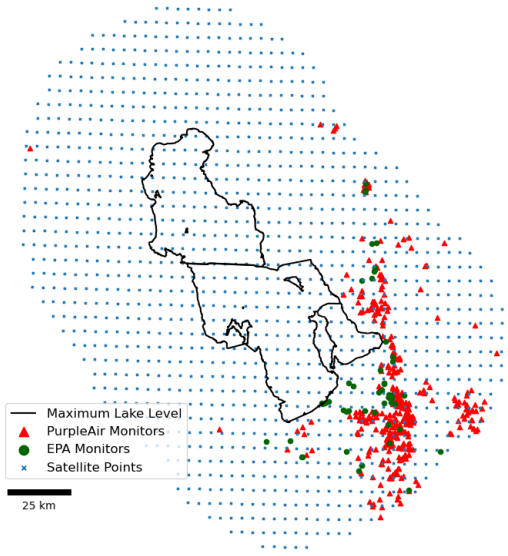
These differences in estimated concentration responses translate into large differences in implied health damages. Using census block-level exposure predictions and standard estimates linking $PM_{2.5}$ to mortality risk, life-years lost, and emergency room utilization, we estimate that the marginal annual health cost of an additional 100 km^2 of exposed lakebed ranges from about \$2.6 million under the HYSPLIT model to roughly \$170 million under the wind-based models, with the near–far model producing an intermediate estimate of about \$113 million. Scaling these marginal damages by observed exposed playa area implies total annual health costs from current desiccation on the order of \$35 million to more than \$2.3 billion per year. Even the lower end of this range is comparable to or exceeds current annual mitigation expenditures, while central estimates are an order of magnitude larger. Taken together, these results indicate that all approaches point to substantial air-quality and health consequences from lake decline, strengthening the economic case for water conservation and lake-stabilization policies.

2 Data

2.1 Air Pollution

We use three alternative, commonly used data sets to measure air pollution changes. The first is readings from pollution monitors operated by the US Environmental Protection Agency (EPA), which are known to provide highly accurate, local air pollution measurements over a relatively sparse monitor network (as shown in Figure 1). Second, we use readings from privately owned PurpleAir pollution monitors, which are generally less accurate than the EPA monitors but are more prevalent leading to a thicker network. Third, we use satellite-derived pollution measurements from van Donkelaar et al. (2024), which provides the most comprehensive spatial coverage but may have limited accuracy for detecting air quality changes arising from lake desiccation. We compare our model results across all three data sets to better understand the trade-offs between accuracy and spatial coverage in the context of lakebed particulate pollution.

Figure 1: Map of Pollution Sampling Points



Notes: Figure plots the subsample of pollution sampling points that are located within 50 km of the lake. The lake boundary is shown at its total maximum extent, at 4,200 ft elevation.

2.1.1 EPA Monitors

We collect daily, 24-hour average concentrations of $PM_{2.5}$ and PM_{10} from the network of EPA managed monitors. We initially gather all measurements available from January 1, 1980 through December 31, 2024 for the subset of monitors located in Utah and the nearby surrounding states[1]. We then trim the distributions of $PM_{2.5}$ and PM_{10} from this sample at the 0.5 and 99.5 percentile to remove any extreme outliers. We next remove observations generated by monitors that are more than 300 km away from the boundary of the Great Salt Lake or occur before 2017. Our final sample, as shown in Table 1, consists of 274,530 observations from 98 monitors.

2.1.2 PurpleAir Monitors

PurpleAir monitors are commercially available for at-home pollution monitoring, and upload readings to a publicly available data repository. From this data we collect monitor-level, daily average measurements for $PM_{2.5}$, PM_{10}, and PM_1 from January 1, 2016 through December 30, 2024 for the subset of outdoor monitors located within 300 km of the Great Salt Lake boundary. Because the data is crowd-sourced and not subject to data quality reviews, we follow guidelines from the EPA to identify and remove observations with data quality concerns, as well as apply a correction for overstated levels at high $PM_{2.5}$ concentrations (Barkjohn, Clements, and Holder, 2022).[2] To our knowledge there is not a commonly accepted correction of PM_{10}. We next remove measurements with particulate measures over $1{,}000\mu g/m^3$, and trim the top and bottom 0.5% of the remaining distributions. We also remove the small set of observations occurring before 2017. This full process results in about 9% of the raw observations being removed from the sample, leaving 605,220 observations from 540 monitors.

[1] Selected surrounding states consist of Nevada, Idaho, Wyoming, and Colorado

[2] Each PurpleAir monitor reports two estimates of each pollutant. The EPA guidelines identify data from a monitor as being valid if the two measurements for $PM_{2.5}$ are either within $5\mu g/m^3$ or 70% of each other (Barkjohn, Clements, and Holder, 2022)

Table 1: Pollution Sampling Point Statistics

	EPA	Purple Air	Satellite
Observations	274,530	605,220	2,690,506
Unique Points	98	540	14,783
Sample Duration	Daily	Daily	Biweekly
Mean $PM_{2.5}$	6.87	6.51	5.44

Notes: Table presents statistics from each pollution sample. Unique Points denotes the number of unique sampling locations in the data set. Sample Duration denotes the temporal availability of pollution measures, within an unbalanced panel framework for the Purple Air and EPA datasets. Mean $PM_{2.5}$ and Mean PM_{10} measure the average pollutant concentrations ($\mu g/m^3$) over the full available sample.

2.1.3 Satellite Measures

We collect biweekly average satellite derived pollution measurements for $PM_{2.5}$ and dust concentrations, available from van Donkelaar et al. (2024). This data is available at a gridded spatial resolution of $0.01° \times 0.01°$ from January 1, 2000 through December 31, 2024. This data obtains estimates of on-ground particulate concentrations by using a combination of aerosol optical depth combined with simulation chemical transport models and ground-based monitors.[3]

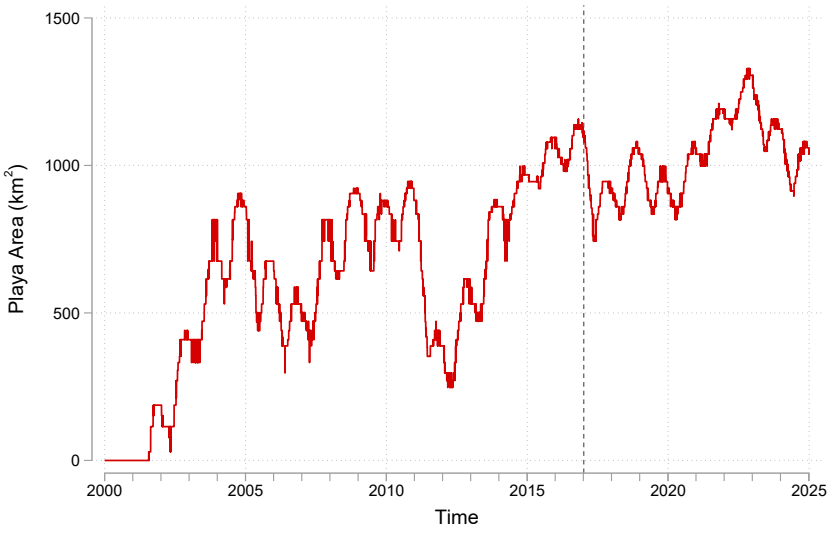
We convert the gridded spatial reference to a point-based dataset to align with the structure of the other data sets. We first construct a $0.05° \times 0.05°$ grid over the sample area. We then define an observation point to be the center of a grid cell, and assign biweekly pollution measurements that are the average of the gridded pollution measurements within the relevant cell. We remove any observations that are located further than 300 km away from the lake and occur before 2017. The result is a sample of about 2.7 million observations for 14,783 unique points.

2.2 Playa Area

We use bathymetric charts to spatially map changes in playa area over time (Tarboton and Merck, 2023). To calculate the corresponding exposed playa area we pull the histories of

[3]Aerosol optical depth from multiple satellite instruments (MODIS/Terra, MODIS /Aqua, MISR/Terra, SeaWiFS/SeaStar, VIIRS/SNPP, and VIIRS/NOAA20) and their respective retrievals (Dark Target, Deep Blue, MAIAC) [] combined with simulation (GEOS-Chem) based upon their relative uncertainties as determined using ground-based sun photometer (AERONET) observations to produce geophysical estimates that explain most of the variance in ground-based $PM_{2.5}$ measurements (van Donkelaar et al., 2024)

Figure 2: Playa Area Over Time



Notes: Figure shows playa area over time between 2000 and 2025 calculated from USGS water level gauges. The vertical dashed line denotes 2017, the start of the PurpleAir pollution sample.

daily water levels since 1990 for two water level gauges in the lake, one in the north half and one in the south.[4] These elevation measures are then mapped to total lake surface area following the crosswalks documented in Baskin (2005) and Baskin (2006).[5] Total playa area is then calculated as the difference between lake surface area on a given day t and the maximum possible lake area (3,613 km^2).

$$\text{Playa Area}_t = \text{Maximum Possible Surface Area} - \text{Lake Surface Area}_t \tag{1}$$

The evolution of playa area over time is shown in Figure 2. Overall, total playa area has increased over time, and exhibits significant year-to-year fluctuations.

[4]Construction of a railroad causeway across the lake in 1959 essentially divided the lake into two halves, north and south, with potentially different water levels. We use water level measures for the south half from the gauge USGS 10010000 Great Salt Lake at Saltair Boat Harbor, UT and for the north half from the gauge USGS 10010100 Great Salt Lake near Saline, UT. These gauges are operated by the US Geological Survey.

[5]Total surface area is constructed by summing the surface area of each lake half.

2.3 Wind Vectors

Variation in a given location's exposure to playa dust is driven in part by wind conditions, which are captured by wind vectors from Copernicus Climate Change Service. These data consist of gridded hourly wind vectors since 1990 to present, and are available at a spatial extent of $0.1° \times 0.1°$. Each vector is characterized by a u- and v-component which reflect the speed of air moving towards the east and north, respectively. The magnitude of the wind vector denotes wind speed, while the angle indicates the direction towards which wind is moving, so that a wind going towards the north would have a Cartesian angle of 90° and a wind going towards the east would have a Cartesian angle of 0°.

2.4 Weather Controls

We use historical PRISM Weather Data to measure daily local precipitation, minimum and maximum temperature, and minimum and maximum vapor pressure deficit (PRISM Group, 2014). This data is available at a gridded resolution of 800m over the years 1981 through 2025.

3 Modeling Alternatives

We compare the marginal effect estimates from four commonly used pollution models with respect to detecting $PM_{2.5}$ concentration changes arising from the desiccation of the Great Salt Lake. The first and simplest model is the "Near-Far" model which compares pollution changes over time for points that are near versus far from the lake (Currie and Walker, 2011; Harris et al., 2024). The second, is the "Hours Downwind" model which compares pollution changes over time for points that spend more time downwind of the lake versus those that spend less (Deryugina et al., 2019; Larkin et al., 2024). The third model, "Angle Downwind", is a variant on the Hours Downwind model with an alternative construction of the downwind measure (Schlenker and Walker, 2016; Kim and Gillingham, 2025). Our last and most computationally intensive model employs a particle transport model (HYSPLIT) to create detailed predictions of dust movements, which we then use as identification in a

differences-in-differences framework (Hernandez-Cortes and Meng, 2023; Abman, Edwards, and Hernandez-Cortes, 2025; Heo, Ito, and Kotamarthi, 2025).

For all models, our main outcome of interest is $PM_{2.5}$ concentrations[6] at monitor p during period t. For the EPA and PurpleAir sample the time period is daily, while for the satellite date the time period is biweekly. All models include a set of 12 environment covariates, denoted E_{pt}, which consist of precipitation, minimum and maximum temperature, minimum and maximum vapor pressure deficit, their squares, and daily average wind speed and its square.

3.1 Near-far

The first model uses a classic near-far differences-in-differences framework, where the first difference is with respect to changes in playa area and the second is with respect to distance from the lake.

$$\begin{aligned} \text{PM}_{pt} = &\sum_{d \in D} \beta_d \mathbb{1}(\text{Distance}_p \in d) \times \text{Playa Area}_t \\ &+ E'_{pt}\gamma + \lambda_1 \mathbb{1}(W_{pt} < 0) W_{pt} + \lambda_2 \mathbb{1}(W_{pt} < 0) W_{pt} + \phi_p + \phi_t + \varepsilon_{pt} \end{aligned} \tag{2}$$

The coefficients of interest are the set of β coefficients, where β_d is the coefficient on the interaction between playa area and an indicator for the distance between the lake and the monitor being in bin d.[7] We define 10 distance bins with cutoffs at 10, 20, 30, 50, 75, 100, 125, 150, 200, 250, and 300 km. In combination, the set of βs flexibly trace out a gradient of the marginal effect of a 100 km^2 increase in playa area over space, relative to the omitted distance bin (250-300km). Our β estimates are conditional on the set of environmental controls, E_{pt}, controls for wind angle based on the definition of W_{pt} in Eq. 5, and point and time fixed effects, ϕ_p and ϕ_t respectively.

While this method is computationally the cheapest, it also imposes the strongest

[6] While existing work suggests that playa particles are generally larger like PM_{10}, the main analysis focuses on $PM_{2.5}$ due to more reliable data. We repeat out models for PM_{10} and dust concentrations in supplemental analyses in the Appendix.

[7] Distance between the lake and a point is measured from the lake boundary at the maximum lake surface area (3,613 km^2).

assumptions. In particular, the model assumes that, conditional on distance from the lake, increases in playa area have spatially uniform impacts on $PM_{2.5}$ concentrations. If wind conditions are the true dispersion mechanism, it is unlikely this would be the case. Therefore, we would expect this model to understate (overstate) the impact of desiccation on $PM_{2.5}$ concentrations for the most (least) exposed areas by ignoring the true spatial specificity of the effects.

3.2 Hours downwind

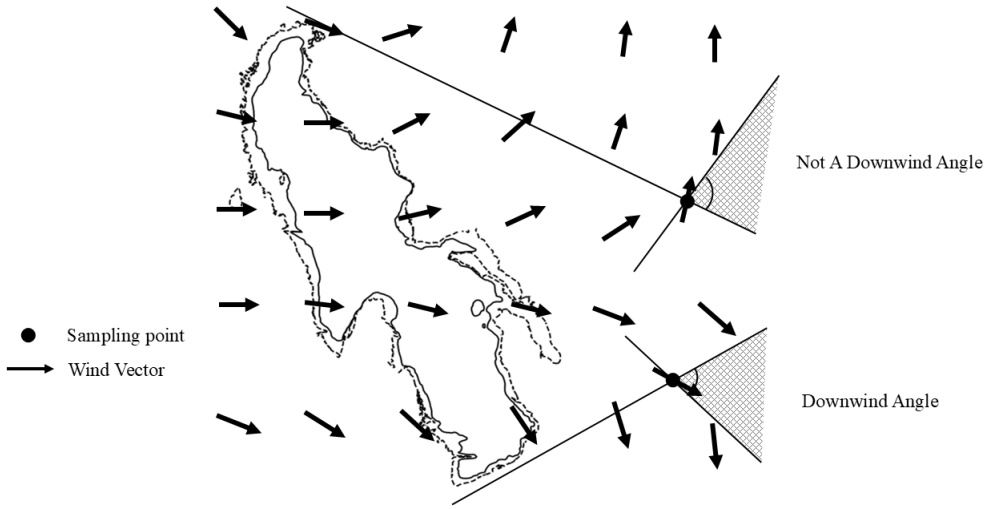
The second model augments the Near-Far model by incorporating wind direction as a determinant of playa dust exposure. We operationalize the hourly wind vectors by creating a daily measure of the number of hours a point spent downwind of the lake polygon (Larkin et al., 2024). To define downwind for a given point p, we identify the set of angles $\mathcal{A}_p$ radiating around the point at which wind blowing linearly in that direction would pass over some part of the lake (at maximum extent) before intersecting the point. This set of angles constitutes the set of potential downwind angles and is denoted by the shaded regions in Figure 3. We then link point p to the hourly wind direction θ_{ph} at that point, and classify p as downwind if the observed wind angle is in the set of downwind angles. We then sum the number of hours for each day that the point is downwind to construct our measure of hours spent downwind of the lake, *Hours Downwind*$_{pt}$. For the satellite-based data, we average the hours downwind over the two week interval to align with the averaged pollution data.

$$0 \leq \text{Hours Downwind}_{pt} = \sum_{h \in t} \mathbb{1}(\theta_{ph} \in \mathcal{A}_p) \leq 24 \tag{3}$$

To estimate the impact of changes in playa area, we incorporate the constructed hours downwind measure into a many-differences framework. The goal of the model is to approximate the true playa dust spatial distribution as closely as possible using a reduced form framework. Since the dust distribution is likely jointly affected by distance from the lake, total playa area, wind direction, and wind speed, our model fully interacts all of these terms.[8] We allow for non-linearities in distance and hours downwind, with $f(\cdot)$ in Equation 4

[8] As a robustness exercise we repeat this analysis on the subsample of non-winter observations, dropping

Figure 3: Stylized Diagram of Hours Downwind Identification



Notes: Figure diagrammatically represents the identification of exposure to playa dust used in the Hours Downwind model. Wind vectors over space are denoted by the black arrows. The example sampling point dots are identified as downwind or not in a given hour based on the wind vector at that point. If the vector falls into the range of downwind angles, $\mathcal{A}_p$ shown as the shaded gray area, then the point is classified as downwind.

representing a quadratic polynomial. Additionally, we include interactions with an indicator for the observation occurring during the winter[9] to capture the seasonal occurrences of temperature inversions which are common to the area around the Great Salt Lake and can impact local air quality.[10] Lastly, we include point (ϕ_p), month ($\phi_{m(t)}$), and year ($\phi_{y(t)}$) fixed effects to account for aggregate shocks to pollution over time and time-invariant local pollution sources. We restrict our analysis sample to points within 100 km of the lake, since the results from the Near-Far model (Figure 7) suggest that there is limited effect beyond

the wind speed and winter measures from Eq. 4. The results shown in Figure A1 are generally similar to the main results.

[9]We define winter as November through March, when inversions are most common (Weller, 2022).

[10]Temperature inversions occur when cold air in the atmosphere gets trapped under a layer of warm air. Inversions are more likely to occur if there is snow, mild winds, and if there are nearby mountains which shield the area. Additionally, inversions can also result in worse air quality due to pollutants being trapped with the cold air (Utah Department of Environmental Quality, 2025). This is a concern for our identification because it means that in winter months playa area (through precipitation changes), wind direction, speed and distance from the lake (through distance from mountains) are all related to both playa dust and inversion-driven pollution exposure.

this point. Standard errors are clustered at the point level.

$$\begin{aligned} \text{PM}_{pt} = & \qquad (4) \\ & [\text{Playa Area}_t \times f(\text{Hours Downwind}_{pt}) \times f(\text{Distance}_p) \times \text{Wind Speed}_{pt} \times \mathbb{1}(\text{Winter}_t)]'\boldsymbol{\beta} \\ & + E'_{pt}\gamma + \phi_p + \phi_m(t) + \phi_y(t) + \varepsilon_{pt} \end{aligned}$$

Our identification comes from comparing changes in $\text{PM}_{2.5}$ concentrations over time across two points that are equidistant from the lake, but with one having spent a larger share of the day downwind from the lake. The idea is that when lake levels are high and there is minimal playa area exposed, the hours spent downwind of the lake should not result in any differential exposure to playa dust. However, when the amount of playa area increases, the wind will now transport the playa dust so that being downwind of the lake leads to exogenously higher concentrations of dust exposure.

The model makes two potentially strong assumptions through the construction of the *Hours Downwind*$_{pt}$ variable. First, the model assumes straight-line winds so that the vector of wind direction at point p can be linearly extended to identify the full path of wind. In reality, air often moves non-linearly through space. Second, the model assumes that the air quality impacts of an hour spent downwind of the lake are homogeneous with respect to the part of the lake that is upwind. However, since the lake shrinks non-uniformly and there is variation in the playa structure over space it is likely that this assumption is incorrectly smoothing variation in dust exposure. Both of these assumptions are likely to bias our estimates towards zero through introducing noise, but are difficult to address without using a more spatially explicit particle transport model.

An additional concern with this model is sufficient power for identification. Using this model entails estimating 80 coefficients excluding fixed effects. Additionally, 65 coefficients are on interaction terms, which generally require larger samples for identification at the same level of precision (Gelman, Hill, and Vehtari, 2020; Leon and Heo, 2009). However this concern is most salient for interactions of binary variables[11], which are relatively few of

[11]The standard error of the coefficient on the interaction of two variables a and b can be written as $\sqrt{\frac{\sigma}{\sum_n a_i^2 b_i^2}}$. In a context where b is binary and evenly distributed over the sample, the standard error

our included variables. Overall, there are reasonable concerns about power with this model, which may favor the use of large N datasets like the satellite data rather than small N data like the EPA monitors.

3.3 Angle downwind

Our third model modifies the Hours Downwind model by redefining how downwind status is measured. For this model, we operationalize the hourly wind vectors by creating a daily measure of the relative distance between the wind direction and the direction that would result in a point being exactly downwind of the lake centroid (Kim and Gillingham, 2025). To construct this measure, we use the following process. First, for every point of interest, p, we identify the angle Θ_p between a vector connecting the lake centroid to the point and a (1,0) vector following the x-axis, where the lake centroid is located at the point (0,0). Θ_p is the angle such that wind blowing in that direction will result in point p being exactly downwind of the lake centroid. Second, we map each point to the 24 hourly wind direction vectors for day t and average them to get a daily average wind direction, denoted θ_{pt}. Third, we calculate the distance between the observed wind direction and the downwind angle using the following equation,

$$W_{pt} = cos(\Theta_p - \theta_{pt}) \tag{5}$$

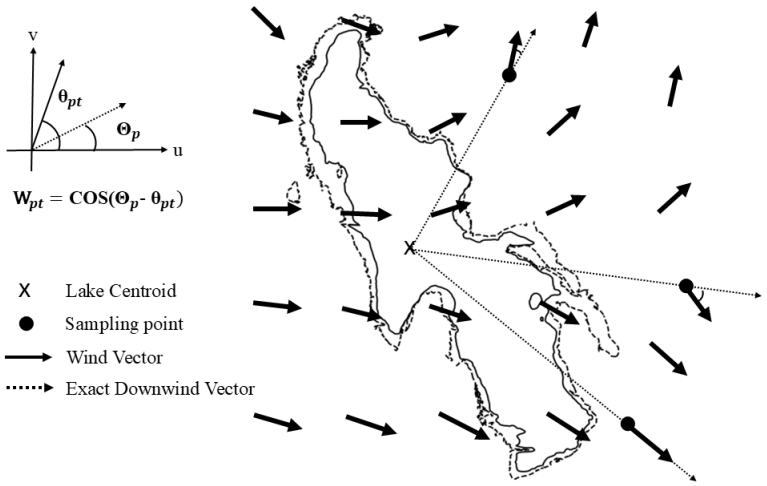
W_{pt} will be equal to one if the wind is blowing such that the point is perfectly downwind from the lake centroid, equal to negative one if the point is perfectly upwind, and approach zero as the wind becomes perpendicular to the downwind vector.

We estimate the impact of changes in playa area by introducing this downwind measure into an almost identical framework as the Hours Downwind model. We again include distance from the lake and its square, total playa area, wind speed, and an indicator for winter in our model, but we now fully interact these with a function of W_{pt}.[12] To account for possible non-linear differences in the effect of wind direction when crossing from some-

becomes $\sqrt{\frac{\sigma}{\sum_{n/2} a_i^2}}$.

[12] As a robustness exercise we repeat this analysis on the subsample of non-winter observations, dropping the wind speed and winter measures from Eq. 6. The results shown in Figure A2 are generally similar to the main results.

Figure 4: Stylized Diagram of Angle Downwind Identification



Notes: Figure diagrammatically represents the identification of exposure to playa dust used in the Angle Downwind model. Wind vectors over space are denoted by the black arrows. For each example sampling point dot, the wind direction at which the point is exactly downwind of the lake centroid is shown as the dashed vector. The cartesian plot highlights the relevant angles of interest which are differenced to create the hourly downwind measure W_{pt}.

what upwind to somewhat downwind, we allow for the coefficients on wind direction to vary with upwind-downwind status. We again include a set of environmental controls, E_{pt}, point, month, and year fixed effects, restrict to points within 100 km of the lake, and cluster standard errors at the point level.

$$\begin{aligned} \text{PM}_{pt} = & \\ & [\text{Playa Area}_t \times \mathbb{1}(W_{pt} \geq 0) W_{pt} \times f(\text{Distance}_p) \times \text{Wind Speed}_{pt} \times \mathbb{1}(\text{Summer}_t)]' \boldsymbol{\beta} \\ & [\text{Playa Area}_t \times \mathbb{1}(W_{pt} < 0) W_{pt} \times f(\text{Distance}_p) \times \text{Wind Speed}_{pt} \times \mathbb{1}(\text{Summer}_t)]' \boldsymbol{\lambda} \\ & + E_{pt}' \gamma + \phi_p + \phi_m(t) + \phi_y(t) + \varepsilon_{pt} \end{aligned} \tag{6}$$

Our identification again comes from comparing changes in $\text{PM}_{2.5}$ concentrations over time across two points that are equidistant from the lake, but now with one point having experienced average wind conditions that are more in line with the direction from the center of the lake. As before, the idea is that when lake levels are high and there is minimal

playa area exposed, the angle of the wind relative to the the lake should not result in any differential exposure to playa dust. However, when the amount of playa area increases the winds coming closer to straight off the lake will transport more playa dust to the point, so that having an average wind direction that is closer to exactly downwind of the lake leads to exogenously higher concentrations of dust exposure.

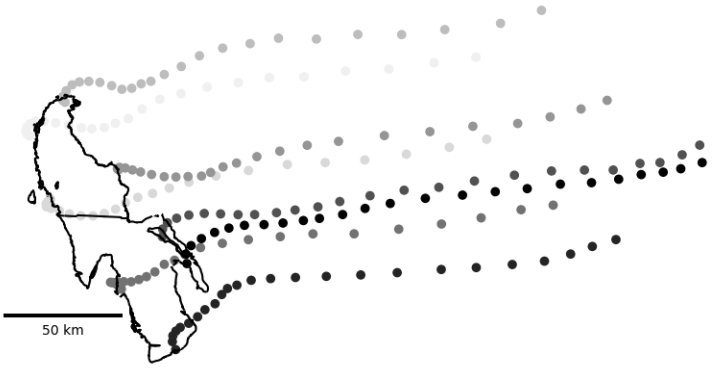
The different definition of downwind exposure results in a new modeling assumption, in addition to some of the same assumptions as the Hours Downwind model. In particular, the model still assumes straight-line winds, when in reality air likely moves non-linearly. Unlike the previous model, this model now assumes that the pollution effect depends semi-linearly on how far the wind angle is from passing over the centroid of the lake. As discussed before, the natural variation in playa composition and area across the full lake bed suggests any pollution impacts would not be uniform across the lake, but there is no evidence that we should expect the lake centroid to be the point that is the most emissive. These assumptions are likely to continue biasing our estimates towards zero.

3.4 HYSPLIT

Our fourth model identifies desiccation driven pollution exposure with a commonly used atmospheric transport and dispersion model, HYSPLIT, operated by the National Oceanic and Atmospheric Administration. This particle transport model uses historic atmospheric conditions to follow particles released from a defined point at ground level over time, returning hourly location coordinates and elevation. To model particle trajectories over our sample, we first create a $0.025^\circ \times 0.025^\circ$ grid across the Great Salt Lake area, and define every grid cell center as a potential emission point. From this set of points, we remove points that are more than 1km away from the lake at its maximum extent (4,200 ft) as well as any points that overlap with the lake below the minimum extent observed in the sample (4,185 ft).[13] We then apply the HYSPLIT model to each emission point to obtain two trajectories for each day, one at 6 AM and one at 6 PM, tracking particles for 24 hours after which

[13]These points are removed for computational purposes. Since they are covered by water during our full sample time, they would never emit particles and so would not contribute to pollution.

Figure 5: HYSPLIT Example Trajectories



Notes: Figure plots the average of the twice-daily HYSPLIT trajectories over the sample time frame for a subset of emission points.

the particles cease to exist. Each resulting trajectory is a set of 25[14] coordinate points per emission event per emission point. This application of HYSPLIT does not capture changes in emission levels from a given source, instead we model how a hypothetical particle emitted from a given point would move through space over time.[15]

The central idea with HYSPLIT is that the modeled particles are a scaled reflection of true particles that are being transported from the lake bed to nearby areas, where they act as PM pollution. As lake levels decline, more modeled and real particles are emitted. However, there are two factors that result in an imperfect correlation between playa area and the measure of total particle emissions that we are interested in (Figure A4). First, not all newly emitted particles are relevant for pollution measurements, for example atmospheric conditions may push particles sufficiently high into the atmosphere so that they are irrelevant for on-the-ground pollution measurements. Second, geographic asymmetry in how the lake shrinks over space and time can drive variation in the number of revealed emission points per unit of playa area.

While HYSPLIT allows us to model changes in pollution relevant particles as playa area changes, it does not explicitly translate particle changes into meaningful changes in pollution. Instead, to estimate the relationship between exposure to the modeled particles and

[14]Inclusive of emission coordinates at hour 0.

[15]A subsample of average trajectories is shown in Figure 5. The trajectories align in an expected way with average wind patterns over the same time frame, shown in A3.

changes in measurable $PM_{2.5}$ pollution we incorporate our modeled particles into a regression model. For each day t, we calculate the number of emitted particles, *Total Particles*$_t$, as the number of modeled particle trajectory coordinates excluding those that are over 1 km in height of that were emitted from points that are covered by water at time of emission. For each pollution monitoring point p, we then calculate the share of particles that occur within a 2.5 km radius buffer around the point on day t.[16]

$$\text{Particle Share}_{pt} = \frac{\sum_i \mathbb{1}(\text{In Buffer})_p}{\text{Total Particles}_t} \tag{7}$$

To identify the impact of increasing total particles as lake levels decline, we interact the particle share term with log of total emitted particles.[17] Our previous models used playa area as a proxy for total emissivity, but due to the specificity of HYSPLIT we are able to explicitly use total emitted particles instead of playa area, reducing measurement error.

$$\text{PM}_{pt} = \alpha\text{Particle Share}_{pt} + \beta ln(\text{Total Particles}_t) \times \text{Particle Share}_{pt} + E'_{pt}\gamma + \phi_p + \phi_t + \varepsilon_{pt} \tag{8}$$

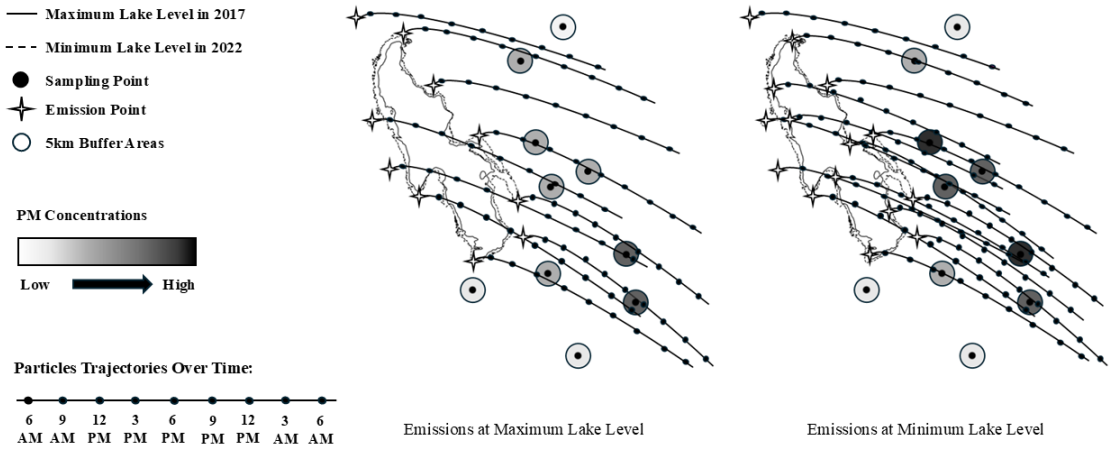
Our main specification again includes a set of environmental controls, point and calendar month fixed effect to account for underlying spatial and temporal differences in pollution unrelated to the lake. We restrict to points within 100 km of the lake and cluster standard errors at the point level.

The idea behind this differences-in-differences approach is that we are comparing pollution across more and less exposed points as the level of exposure changes with lake levels. *Total Particles*$_t$ captures percent changes in the total amount of windblown dust over time as more playa area becomes exposed and emits more dust. *Particle Share*$_{pt}$ operates analogously to the upwind/downwind measures above by identifying the concentration of dust arriving in a specific location. A stylized diagrammatic representation of this model is shown in Figure 6. We would expect that for a given number of emission points, points intersected by more particle paths would be subject to worse pollution, α is positive. As lake levels change, the number of emission points and subsequent particle paths mechanically

[16] We use particle share rather than raw counts to make our estimated impacts independent of the arbitrarily chosen number of initial points.

[17] We use the log of total particles for easier interpretability of the coefficient estimate.

Figure 6: Stylized Diagram of HYSPLIT Identification



Notes: Figure diagrammatically represents the identification of Eq. 8. Points from which modeled particles are emitted are reflected by the stars, while points where pollution is measured are denoted by the dots within the buffer regions. Particle trajectories are traced out with example particle coordinate points along the trajectory paths. *Particle Share*$_{pt}$ is calculated by counting the number of particle coordinate points in a given buffer and dividing by the total number of particle coordinates. The left hand figure reflects an emission scenario when the lake is at the maximum level observed in the sample. Points surrounded by buffers with higher shares of particle coordinates have relatively higher PM concentrations (positive α). The right hand figure reflects an emission scenario when the lake is at the minimum level observed in the sample. There are more emission points than the left figure, and therefore more particle coordinate points. Buffers with higher shares of particle coordinates have even higher PM concentrations than the left hand figure (positive β).

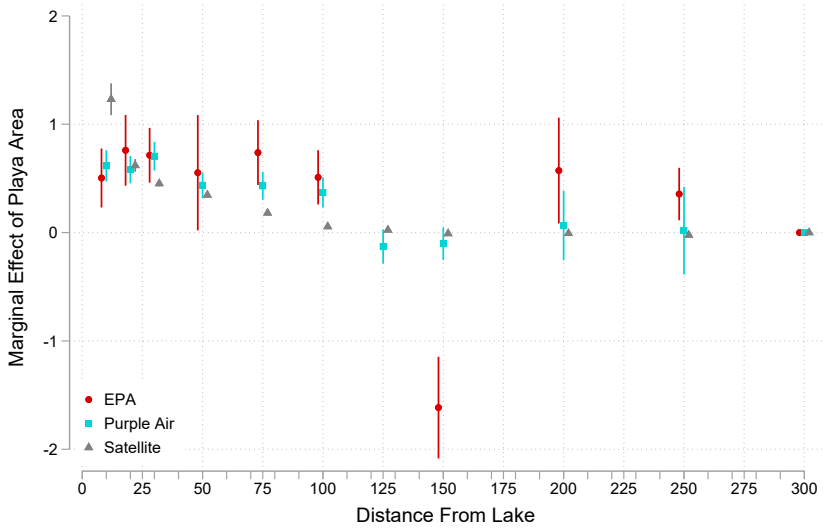
increases, reflective of increased true emissions from newly exposed playa area. Then during times of high total emissions, we would expect a larger share of particles to reflect a larger increase in real particles and pollution, β is positive.

4 Results

4.1 Near-far

We start with the simplest model, the Near-Far differences-in-differences, which generates consistent predictions across the three pollution samples of meaningful increases in $PM_{2.5}$

Figure 7: Near-Far Marginal Effect Estimates



Notes: Figure plots the marginal effect estimate gradient from Eq. 2 over distance from the lake. Marginal playa effect is interpreted as the $\mu g/\text{m}^3$ increase in $\text{PM}_{2.5}$ arising from a 100 km^2 increase in playa area, relative to the effect at 300 km from the lake. 95% confidence intervals for standard errors clustered at the point level are shown as vertical lines.

from increased playa area exposure. The results of the three estimation processes are shown in Figure 7, which plots the marginal effect point estimates (the set of β coefficients from Equation 2) and their 95% confidence intervals. Perhaps most striking in the figure is how well the point estimates align across the three samples. All samples predict a 0.6 to 0.7 $\mu g/\text{m}^3$ average increase in $\text{PM}_{2.5}$ per 100 km^2 increase in playa area within 30 km of the lake. Additionally, all of the samples show a non-zero marginal effect extending out to about 100 km away from the lake.

However, across the three samples there are some important differences in the marginal effect estimates. First, the satellite data shows a very smooth decline over space towards a null-impact while the PurpleAir, and to a lesser extent EPA, data document a more discrete step down after 100 km away from the lake. This may be driven by differences in the mechanics of how pollution is being measured (i.e. directly measured vs modeled). Second, and unsurprisingly, there are distinct differences in the statistical precision of the point estimates, with the small EPA sample being relatively noisy and the large satellite-based sample being highly precise.

As a first pass at modeling the pollution impacts from lake desiccation, the Near-Far model documents adverse impacts of lake desiccation on air quality, with low computational costs. The spatial extent of these impacts is large, extending out to about 100 km away from the lake. Additionally, even though the main effect estimates are likely biased towards zero due to the spatial smoothing inherent in the model, the impact within 30 km of the lake is still quite large. Compared to the sample average $PM_{2.5}$ concentrations (Table 1), the marginal effect of a 100 km^2 increase in playa area translates into about a 10% increase in $PM_{2.5}$ concentrations.

In addition to this main analysis, we include results from two alternative specifications in the appendix. First, we repeat the main analysis extending the time frame of the satellite and EPA samples to include all data since 2000 (Figure A5). We find a roughly similar gradient as the main results for the EPA sample, but a significantly steeper gradient with the satellite data, returning positive effects only within 10 km of the lake. Second, we examine the gradient for PM_{10} and dust concentrations (Figure A6). We find a roughly similar, though significantly noisier, gradient for the EPA and PurpleAir PM_{10} samples, with coefficient magnitudes similar to those estimated for $PM_{2.5}$. The satellite measured dust sample shows negligible increases in pollution within 50 km of the lake.

4.2 Hours downwind

Incorporating wind variation into our identification for the Hours Downwind model returns marginal effect estimates that are more spatially diverse and have a larger maximum effect, peaking at over a 2 $\mu g/m^3$ increase. Figure 8 depicts the marginal effect gradient, estimated from Eq. 4 for non-winter periods, as a function of distance from the lake and hours spent downwind. For both the EPA and PurpleAir samples, we find that close to the lake (within 50 km) the marginal effect of playa area increases with time spent downwind. This confirms that close to the lake more time spent downwind means greater transport of dust as more playa area becomes exposed. However, further from the lake we find the marginal effect is increasing up to about 10 hours and then decreasing with subsequent time downwind. This could capture a "clearing out" dynamic where persistent winds push out all pollution from an area, offsetting any increase that would occur from exposed playa, leading to a net zero

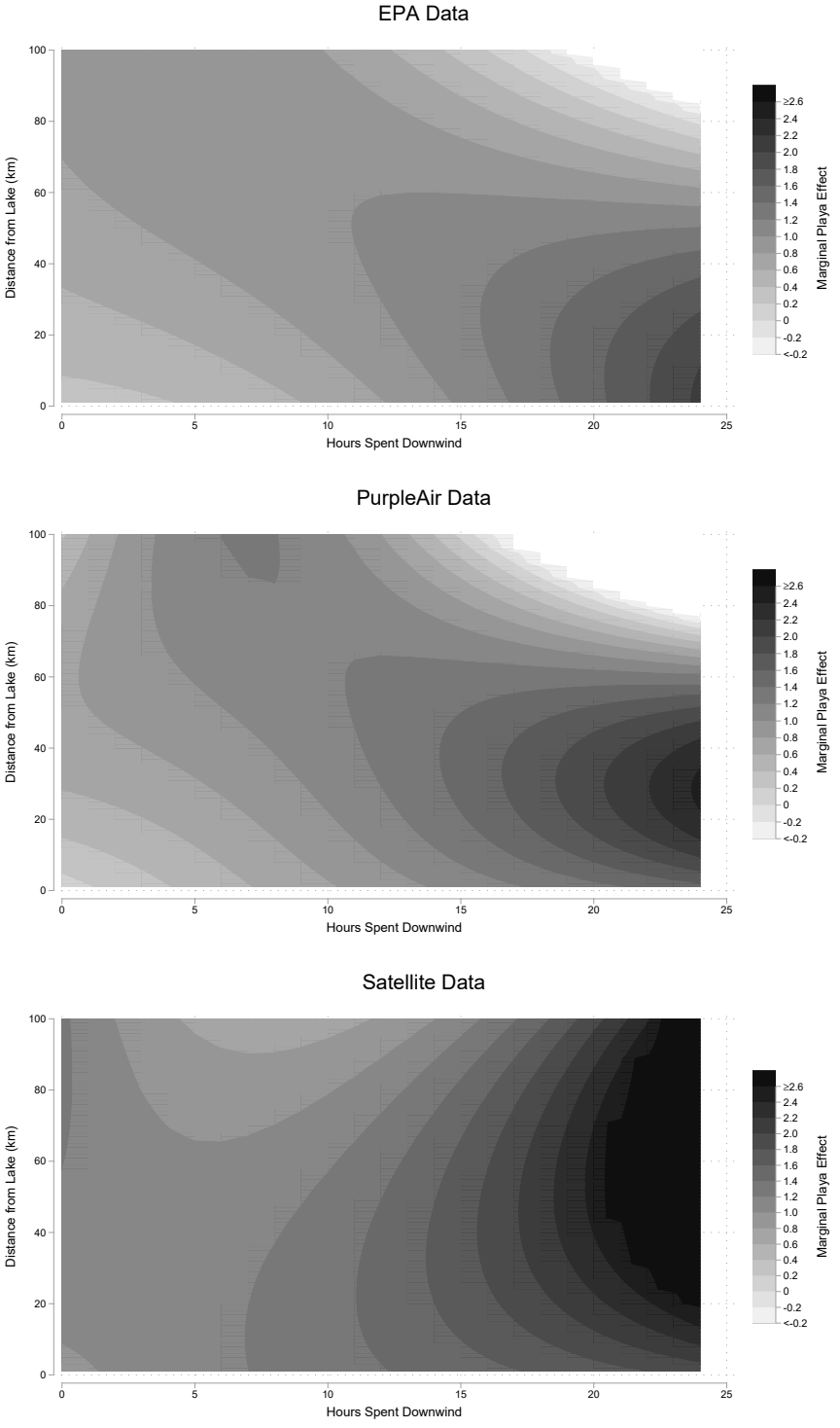
effect. Figure A7 documents this relationship in the raw data, showing $PM_{2.5}$ concentrations increase as a function of hours spent downwind before starting a rapid decline between 5 and 10 hours.

Alternatively, when holding the number of hours spent downwind fixed, we find that for under 15 hours the largest marginal effects are concentrated further rather than nearer to the lake. We believe that this is a residual of our definition of downwind. A point is considered downwind of the lake if the wind angle is in the set of angles $\mathcal{A}_p$ (Eq. 3). Mechanically, the further a point is from the lake, the smaller the set of downwind angles becomes (Figure A8). Therefore, points further from the lake will have less variation in wind direction for a given time spent downwind than points closer to the lake. It seems likely then that this more stable wind pattern would equate to more reliable transport of playa dust to the further point for a fixed amount of time documented as downwind.

Using the satellite data, we again see time spent downwind increases $PM_{2.5}$, though there is less spatial variation in effect. This difference compared to the other datasets may be a result of the biweekly temporal aggregation reducing the available identifying variation. In the satellite sample, the 95^{th} percentile of hours spend downwind is 14 hours, in contrast with the 95^{th} percentile in the EPA and PurpleAir samples of 17 hours. The somewhat condensed distribution of the independent variable could be resulting in weak identification of the marginal effect for higher number of hours spent downwind, the range at which the most notable variation in marginal effects occurs with the EPA and PurpleAir samples.

Overall, the Hours Downwind model results indicate that desiccation increases particulate matter exposure heterogeneously, with consistently downwind locations closest to the lake experiencing severe increases in pollution. Two limitations of this model appeared during our analyses. First, temporal aggregation of data results in a limited support for identification, potentially obfuscating important and interesting spatial heterogeneity. Second, in the context of the Great Salt Lake there are endogeneity concerns with respect to local atmospheric inversions (Section 3.2). Plotting the marginal effect estimates for winter shows very dissimilar effects both across samples and relative to the non-winter results (Figure A9). In combination, these results indicate that the Hours Downwind model is inappropriate to use with temporally aggregated data, or in contexts where wind conditions are correlated

Figure 8: Hours Downwind Marginal Effect Estimates



Notes: Figure plots the marginal effect estimate gradient from Eq. 4 over distance from the lake and the number of hours spent downwind. Marginal playa effect is interpreted as the $\mu g/\mathrm{m}^3$ increase in $\mathrm{PM}_{2.5}$ arising from a 100 km^2 increase in playa area. The calculation assumes a non-winter period and a wind speed of 1.67.

with other climatic phenomena.

4.3 Angle downwind

The Angle Downwind model similarly shows significant increases in $PM_{2.5}$ concentrations downwind from the lake. We again map the estimated marginal effect over space in Figure 9, plotting the marginal effect of a 100 km^2 increase in playa area, over space relative to the lake. The x-axis indicates the distance in kilometers east from the lake, while the y-axis reflects the distance north, with the lake collapsed into the origin point.[18] We assume a non-winter period with wind at all points blowing due east, parallel with the x-axis.

Across all three panels, Figure 9 shows the alternative samples returns very similar marginal effect estimates. All capture a plume like dispersion of particulates directly downwind of the lake, with the largest increases in particulate exposure are concentrated within about 30 km downwind of the lake. Within 30 km downwind, the peak increases in $PM_{2.5}$ concentrations from a 100 km^2 increase in playa area are between 1.8 $\mu g/m^3$ (satellite data) and 2.28 $\mu g/m^3$ (PurpleAir data). While very similar, the satellite data does stand out as having relatively less variation in estimated marginal effect over space, again likely due to reduced identifying variation. In the satellite data, the sample standard deviation of observed wind angle is 0.28, while it is about 0.47 in the daily samples.[19]

The Angle Downwind model reaffirms the previous model results, indicating that desiccation leads to significant increases in $PM_{2.5}$ concentrations for areas downwind and close to the lake. For robustness, we also map the estimated marginal effects during winter (Figure A10). We find increased pollution concentrations directly upwind of the lake, again raising concerns about exogeneity.

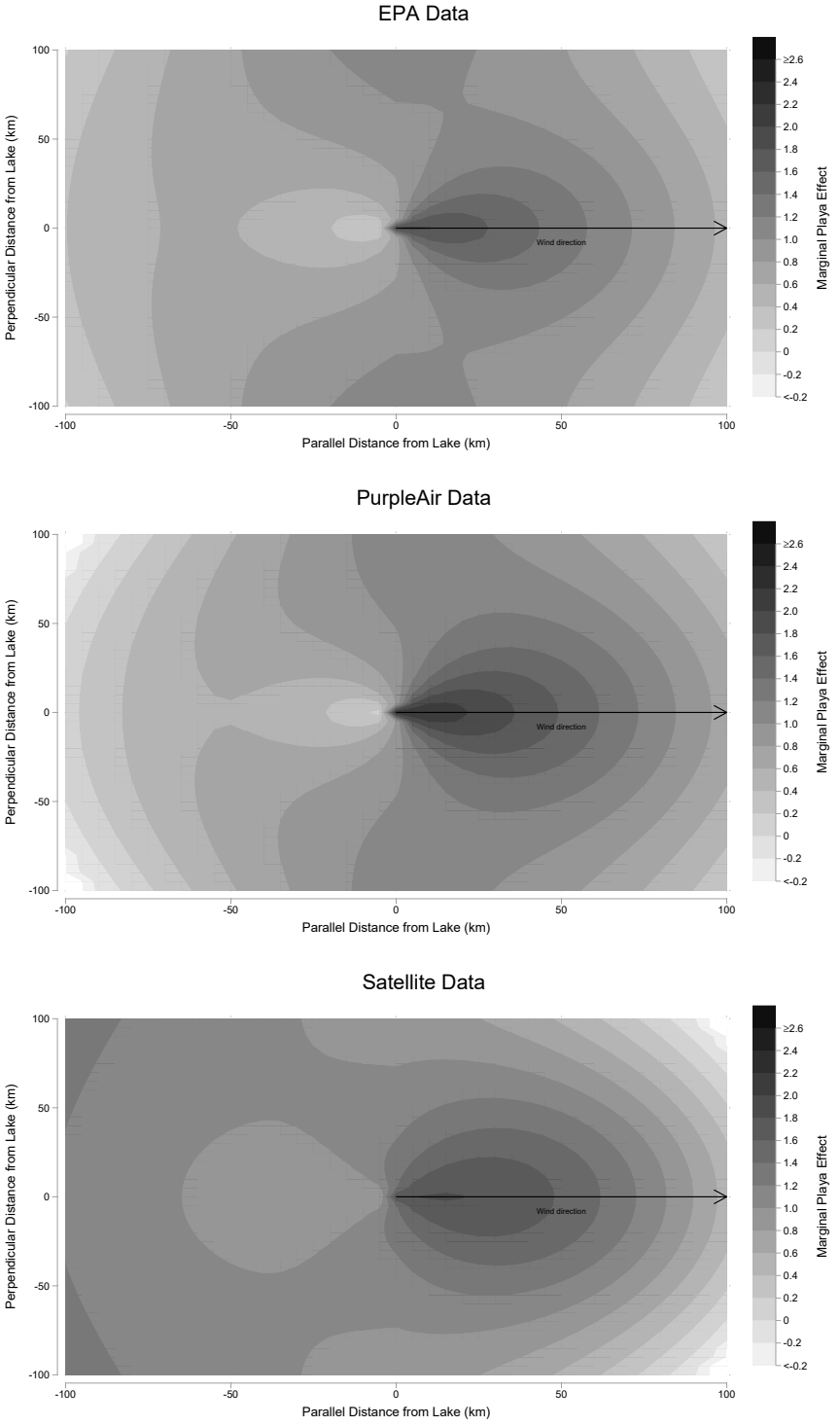
4.4 HYSPLIT

Our analysis on the relationship between HYSPLIT particles and pollution shows a positive and significant interaction between $Total\ Particles_t$ and $Particle\ Share_{pt}$, indicating the

[18] A point that is due north of the lake centroid and 10 km away from the lake edge would be located at (0,10). A point that is due east of the lake centroid and 10 km away from the lake edge would be located at (10,0).

[19] The observed wind angle is bounded between -1 and 1.

Figure 9: Angle Downwind Marginal Effect Estimates



Notes: Figure plots the marginal effect estimate gradient from Eq. 6 over location relative to the lake. Distance north is shown on the y-axis, and distance east on the x-axis. The lake is located at the point (0,0). Marginal playa effect is interpreted as the $\mu g/\mathrm{m}^3$ increase in $\mathrm{PM}_{2.5}$ arising from a 100 km^2 increase in playa area. The calculation assumes a non-winter period, a wind direction of going due-east, and a wind speed of 1.67.

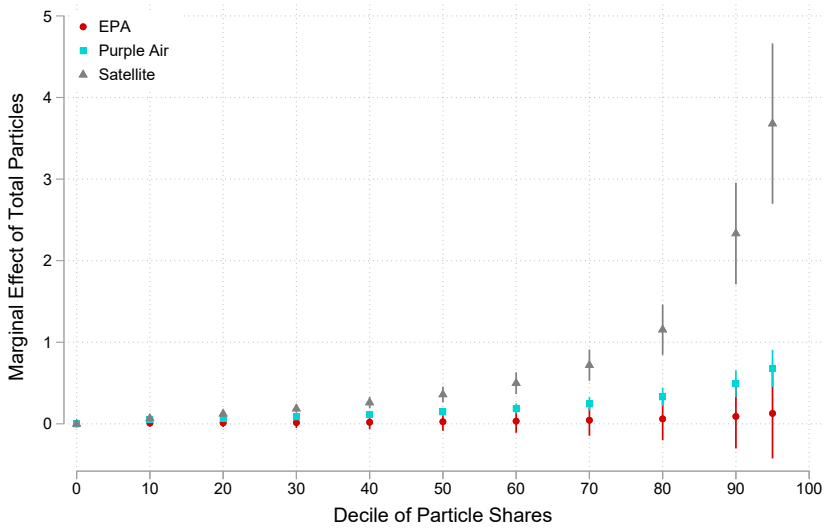
declining lake levels lead to higher $PM_{2.5}$ concentrations in exposed areas. To visualize the relationship, Figure 10 plots the estimated coefficient on the interaction term scaled by the relevant share of particles for each decile of the particle share distribution, conditional on non-zero particle shares (point estimates shown in Table A1).[20] The figure shows that, for all datasets, the estimated marginal effect of *Total Particles*$_t$ is highest in the upper end of the distribution of *Particle Share*$_{pt}$. Areas which are subject to relatively more modeled particles from the lake in a given period experience larger increases in $PM_{2.5}$ concentrations during high total particle (low lake level) times than areas that are relatively less exposed.[21] For example, with the PurpleAir sample, at the 20^{th} percentile a 1% increase in total particles results in a 0.06 $\mu g/\text{m}^3$ increase in $PM_{2.5}$ concentrations, while at the 80^{th} percentile a 1% increase in total particles results in a 0.33 $\mu g/\text{m}^3$ increase. With respect to space, areas closest to the lake are more likely to have higher particle shares (Figure A11), meaning areas closer to the lake will have larger increases in pollution with more total particles, in line with the three previous models.

Directly interpreting the impact of lake desiccation with this model is muddled by the use of total particles in the estimation, rather than proxying for this change with playa area. However, we can regress total particles on playa area to get a coarse approximation of a first stage relationship for comparative purposes. Across the three samples, we estimate that a 100 km^2 increase in playa area leads to an average increase in total particles of 0.1 log points (Table A1). Scaling our PurpleAir results, this implies that at the 20^{th} percentile of particle share, a 100 km^2 increase in playa area would result in about a 0.006 $\mu g/\text{m}^3$ increase in $PM_{2.5}$, while at the 80^{th} percentile, it would be about a 0.033 $\mu g/\text{m}^3$ increase. These results are significantly smaller than the estimates from the previous models.

[20] Instead of the 100^{th} percentile of particle shares we show the 95^{th} percentile, since outliers above the 95^{th} percentile make the graph difficult to read.

[21] Note that the model returns a linear relationship between *Particle Share*$_{pt}$ and $PM_{2.5}$ conditional on *Total Particles*$_t$, however the skewed distribution of *Particle Share*$_{pt}$ results in a non-linear relationship over percentiles of *Particle Share*$_{pt}$.

Figure 10: HYSPLIT Marginal Effect Estimates



Notes: Figure plots the marginal effect estimate gradient from Eq. 8 over percentile of particle shares. The marginal effect is interpreted as the $\mu g/\text{m}^3$ increase in $PM_{2.5}$ arising from a 1% increase in total particles emitted, given particle shares in the buffer. Clustered standard errors are denoted by the vertical bars.

5 Modeling Comparison

Across all modeling approaches and datasets there are distinctive commonalities. With respect to modeling approaches, all four methods result in broadly similar spatial distributions of playa dust exposure, predicting significant increases in $PM_{2.5}$ close to the lake (generally within 30 - 50 km). With respect to data sample, the EPA and PurpleAir monitors result in very similar parameter estimates across all except the HYSPLIT model. The satellite data produces generally similar, though more spatially homogenous results, compared to the other two. Of all of the models, the HYSPLIT results are much more sensitive to analysis sample selection than the others.

An important difference across the four models is the magnitude of estimated marginal effect of a 100 km^2 increase in playa area. For the Angle and Hours Downwind models, the marginal effect estimates are quite similar: peaking around $2.2\mu g/\text{m}^3$ for the most exposed areas, with meaningful increases of around $1\mu g/\text{m}^3$ for moderately exposed areas. It is interesting to note that these point estimates align with similar estimates for the Salton Sea, placing the marginal effect of a 100 km^2 increase in playa area at $2.22\mu g/\text{m}^3$ (Jones

and Fleck, 2020).[22] The Near-Far model on the other hand returns a smaller marginal effect estimate, peaking between 0.6 and $0.7\mu g/\text{m}^3$. This attenuation relative to the Angle and Hours Downwind models is likely a result of the reduced spatial specificity of identifying variation employed in the model. Lastly, the HYSPLIT model also returns a smaller marginal effect estimates based on the back-of-the-envelope conversion, peaking at $1\mu g/\text{m}^3$ for the most exposed locations.[23]

To underscore the importance of these documented discrepancies in predictions from our four commonly used models, we use the models to calculate a coarse "cost of desiccation". For this exercise we use the model parameters and observed environmental conditions to calculate daily marginal effects for each census block across Utah, for every day in 2023.[24] We then convert these effect estimates into monetary costs with estimates from Deryugina et al. (2019) for the value of health damages arising from $PM_{2.5}$ exposure through reductions in life years and increases in ER spending and visits.[25] Summing each of these block-day level costs returns our estimated cost of desiccation for each model.

This exercise shows that alternative model selections can lead to substantially different cost estimates, as shown in Table 2. The HYSPLIT model stands out as estimating the lowest marginal health cost of playa area, at $2.6 million, while the Hours and Angle Downwind models return nearly identical, large estimates around $172 million. These marginal costs reflect the aggregate health cost of a 100 km^2 increase in playa area. To understand the scale of the full situation, we linearly extrapolate out our marginal cost predictions to reflect the amount of exposed playa as of January 2025, 1,328 km^2. These values, shown in the second panel of Table 2 show a total desiccation cost ranging between $35 million and $2.3 billion annually.

[22] Jones and Fleck (2020) estimate a linear OLS model, regressing county level $PM_{2.5}$ concentrations on playa area conditional on a set of environmental controls. They measure $PM_{2.5}$ concentrations with the satellite dataset used in our analyses, aggregated to an annual level.

[23] Note that for some locations with the largest shares of particles ($> 95^{\text{th}}$ percentile) the estimated marginal effects can be extremely large depending on the estimation sample, though this result seems to be driven primarily by a few outliers with large particle shares.

[24] We estimate the marginal effect at the block centroid.

[25] Our calculations use the authors' estimates for the increase in life years lost (2.99 per million), ER visits (2.7 per million), and ER spending ($16,400 per million) per $1\mu g/\text{m}^3$ increase in $PM_{2.5}$ along with an assumed value per life-year of $100,000. For a given block b on day t we calculate the cost of playa dust as $\text{Cost}_{bt} = \text{Marginal Effect}_{bt} \times (2.99 \times 100,000 + 2.7 \times 16,400) \times \frac{\text{Population}_b}{1,000,000}$.

Table 2: Estimated Cost of Playa Area

	Near-Far	Hours Downwind	Angle Downwind	HYSPLIT
Marginal Cost				
Cost ($ millions)	113.42	172.71	172.66	2.65
Total Desiccation Cost				
Cost ($ millions)	1,506.2	2,293.5	2,293.0	35.2

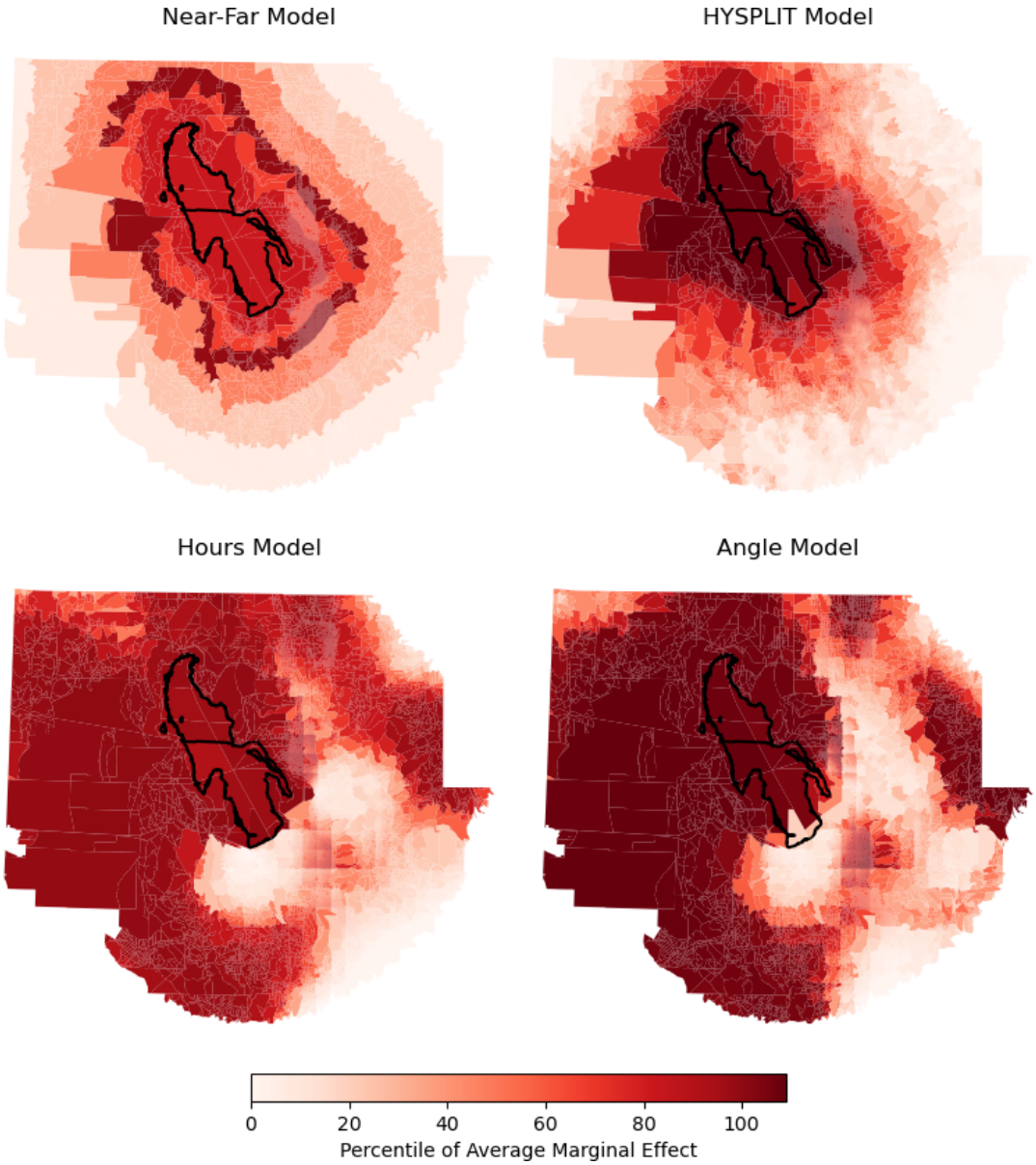
Notes: Table presents estimates of desiccation related health costs. Marginal health costs are calculated by scaling census-block marginal increases in $PM_{2.5}$ by health costs from Deryugina et al. (2019). The total desiccation cost is calculated by scaling marginal costs by the total amount of exposed playa area in January 2025.

The variation in desiccation cost estimates across models depends on both the spatial distribution of modeled playa dust as well as the estimated magnitude of pollution increases. To visualize the variation in spatial distribution predicted by each model, the average marginal effect for each block is mapped in Figure 11. Each map shows the estimated average marginal effect, as a percentile of the distribution generated by the relevant model over all census blocks in Utah. The Near-Far and HYSPLIT models calculate the most severe exposure for blocks quite close to the lake and in a relatively symmetic way around the lake. The Hours and Angle Downwind models instead show the most severe exposure for areas to the northwest of the lake, and relatively little exposure near the southeast side of the lake. Given that population density is relatively high on the southeast side of the lake and low on the northwest, this will dampen some of the aggregate estimated health cost increase under these models, since the worst exposed areas have relatively few people. Therefore, the drastic difference in cost across the four models is driven primarily by the differences in marginal effect magnitude across the models.

6 Cost and Optimality of Abatement

Policy solutions to reduce or eliminate the Great Salt Lake (GSL) as a source of pollution fall into two broad categories: re-watering the lake to cover the playa or mitigating playa dust through physical modification of the playa surface. In reality, the policy outcome may be a combination of both approaches plus the acceptance of some residual dust pollution. To reduce the dimensionality of this problem, we focus on estimating the total costs of approaches

Figure 11: Marginal Effect Estimate Maps



Notes: Figure plots the percentile of the average marginal increase in $PM_{2.5}$ concentrations. Estimates are for 2023. The percentile for a given block is calculated relative to all other blocks under the given model.

laid out in (Great Salt Lake Strike Team, 2026). The report models four scenarios: (i) baseline, no additional inflows; (ii) increase of 250,000 AF of inflows annually; (iii) increase of 375,000 AF; and (iv) increase of 800,000 AF. Changes in inflows are translated into annual lake elevation using hydrologic accounting and lake response relationships as summarized in Figure 21 of the report (Great Salt Lake Strike Team, 2026).

Starting with these elevations, we use lake bathymetry to translate lake elevation into implied changes in exposed playa, which is the focus of our cost analysis

We focus on three categories of cost: health costs related to dust pollution; leasing costs of obtaining water rights to increase inflows; and mitigation costs of modifying GSL plays to make it less emissive. We focus on these costs to put the magnitude of the health costs into context. The inclusion of other environmental costs associated with lake desiccation, such as loss of bird habitat or brine shrimp production, is beyond the scope of the present paper.

HEALTH COSTS

WATER COSTS: The GSL watershed is comprised of three main rivers (Weber, Jordan, and Bear) whose drainage basins cover portions of Utah, Idaho, and Wyoming. In the 2020-2024 period agricultural water depletion in the entire GSL basin averaged 1,551 kAF annually Great Salt Lake Strike Team, 2026. Li and Khan (2025) estimate a discrete choice model of irrigator behavior with random effects using spatially disaggregated cropland rent applied at a 30m resolution using the Cropland Data Layer. Their analysis suggests that fallowing irrigated alfalfa could generate approximately 512 kAF (632 million m^3) of water savings annually in the Utah portion of the watersheds closest to the lake. They recover a distribution of willingness-to-accept (WTA) across all alfalfa pixels, creating a marginal abatement cost curve which we use as a water leasing supply curve.

Li and Khan (2025) estimate the least productive alfalfa farmer would sell water at around $432 per acre-foot and the most productive at $975 per AF. These estimates are likely quite high and represent an upper bound of what farmers would actually require. On-the-ground leasing by the GSL Commissioner's Office is currently taking place at around $300; anectdotally the spot market for water rights is significantly lower than this price altough water right prices are not public record and the market is thin; estimates of marginal value of water in ag in Utah are around $XX/AF. The approach Li and Khan (2025) use is conservative because it incorporates land-use inertia and other unobserved factors affecting land-use decisions into switching costs, which increases the farmers' WTA. Because their MAC curve only covers alfalfa in a portion of the basin, it ends at 512 kAF. We assume additional water, up to 800 kAF, is available at the highest estimated cost (about $975/AF).

7 Conclusion

This research has documented how several commonly used empirical identification strategies and data sources perform at isolating the causal impact of a natural pollution source. We find that the general spatial relationship between pollution and source predicted by the alternative models is relatively consistent across all models. Conditional on model selection, we found that results were relatively invariant to the analysis sample used, opening the way for future research to take advantage of new pollution measuring technologies like community-sourced and satellite data. However, across models the estimated marginal effects varied widely, an important discrepancy for evidence-based policy decisions.

In the particular context of the Great Salt Lake, we estimated that the health costs attributable to desiccation due to worsened air quality are significant, ranging between $35 million and $2.3 billion annually. While the range of these estimates is dramatic, no matter the model used the annual health costs far exceed estimated annual mitigation costs. Current estimates from the Utah Legislature place annual lake mitigation costs at $15 million, after an upfront initial mitigation cost of $1.5 billion (Utah OLAG, 2023). Even accounting for the large initial mitigation cost, all models except the lowest cost estimate indicate net positive values within two years of mitigation. Documentation of the impact of desiccation on air quality, and recognizing the variation in magnitude arising from model selection, are necessary for better informed water policy in the context of the Great Salt Lake.

References

Abman, Ryan, Eric C Edwards, and Danae Hernandez-Cortes (2025). "Water, dust, and environmental justice: The case of agricultural water diversions". In: *American Journal of Agricultural Economics* 107.4, pp. 1041–1058.

Aragon, Fernando M. and Juan Pablo Rud (2021). "Dust and Death: Evidence from the West African Harmattan". In: *American Economic Review* 111.5, pp. 1443–1472. DOI: 10.1257/aer.20191284.

Barkjohn, Karoline, Andrea Clements, and Amara Holder (2022). "ORD Updates: AirNow Fire and Smoke Map". In: US Environmental Protection Agency.

Baskin, Robert L. (2005). "Calculation of Area and Volume for the Sorth Part of Great Salt Lake, Utah". In: pp. 1–6.

— (2006). "Calculation of Area and Volume for the North Part of Great Salt Lake, Utah". In: pp. 1–6.

Borgschulte, Mark, David Molitor, and Eric Yongchen Zou (2024). "Air pollution and the labor market: Evidence from wildfire smoke". In: *Review of Economics and Statistics* 106.6, pp. 1558–1575.

Burke, Marshall et al. (2018). "Health impacts of dust exposure from drying lakes". In: *Nature Climate Change*.

Burke, Marshall et al. (2023). "The contribution of wildfire to PM2. 5 trends in the USA". In: *Nature* 622.7984, pp. 761–766.

Currie, Janet and Reed Walker (2011). "Traffic Congestion and Infant Health: Evidence from E-ZPass". In: *American Economic Journal: Applied Economics* 3.1, pp. 65–90. DOI: https://doi.org/10.1257/app.3.1.65.

Deryugina, Tatyana et al. (2019). "The Mortality and Medical Costs of Air Pollution: Evidence from Changes in Wind Direction". In: *American Economic Review* 109.12, pp. 4178–4219. DOI: https://doi.org/10.1257/aer.20180279.

Flavelle, Christopher (June 7, 2022). "As the Great Salt Lake Dries Up, Utah Faces an 'Environmental Nuclear Bomb'". In: *The New York Times*. URL: https://www.nytimes.com/2022/06/07/climate/salt-lake-city-climate-disaster.html.

Gelman, Andrew, Jennifer Hill, and Aki Vehtari (2020). *Regression and Other Stories*. Cambridge University Press.

Great Salt Lake Strike Team (2026). *Great Salt Lake Data and Insights Summary*. Technical Report. Version 1.0, prepared for the 2026 Utah Legislative Session. State of Utah.

Harris, Lena et al. (2024). "Limited impact of roadway construction and traffic congestion on nearby housing prices". In: *Transport Policy* 157, pp. 1–9. DOI: https://doi.org/10.1016/j.tranpol.2024.07.019.

Heo, Seonmin Will, Koichiro Ito, and Pao Kotamarthi (2025). "Do environmental markets cause environmental injustice? Evidence from California's carbon market". In: *The Review of Economics and Statistics*, pp. 1–45. DOI: https://doi.org/10.1162/rest_a_01581.

Hernandez-Cortes, Danae and Kyle C. Meng (2023). "Do environmental markets cause environmental injustice? Evidence from California's carbon market". In: *Journal of Public Economics* 217. DOI: https://doi.org/10.1016/j.jpubeco.2022.104786.

Jones, Benjamin et al. (2015). "Drying lakes and health impacts in Morocco". In: *Proceedings of the National Academy of Sciences*.

Jones, Benjamin A. and John Fleck (2020). "Shrinking lakes, air pollution, and human health: Evidence from California's Salton Sea". In: *Science of The Total Environment* 712. DOI: https://doi.org/10.1016/j.scitotenv.2019.136490.

Jones, Benjamin A., Jingjing Wang, and John Fleck (2025). "Sending Agricultural Water to the Salton Sea to Improve Public Health? An Integrated Agri-Hydro-Health Economic Analysis". In: *Journal of the Association of Environmental and Resource Economists* 13.2. DOI: 10.1086/737530. URL: https://www.journals.uchicago.edu/doi/10.1086/737530.

Kim, Seung Min and Kenneth T. Gillingham (2025). "Air pollution and solar energy: evidence from wildfires". In: *Journal of the Association of Environmental and Resource Economists* 12.2, pp. 493–526.

Krasnov, H. et al. (2014). "Contribution of dust storms to PM10 levels in an urban arid environment". In: *Atmospheric Research*.

Larkin, Andrew et al. (2024). "High traffic roads and adverse birth outcomes: comparing births upwind and downwind of the same road". In: *American Journal of Epidemiology* 193.12, pp. 1720–1728. DOI: https://doi.org/10.1093/aje/kwae120.

Legislative Auditor General, Office of the (2023). *High-Risk List: Identifying and Mitigating Critical Vulnerabilities in Utah*. 2023-10, pp. 1–128.

Leon, Andrew C and Moonseong Heo (2009). "Sample Sizes Required to Detect Interactions between Two Binary Fixed-Effects in a Mixed-Effects Linear Regression Model". In: *Computational Statistics Data Analysis* 53.3, pp. 603–608. DOI: https://doi.org/10.1016/j.csda.2008.06.010.

Li, Man and Asif Ahmed Khan (2025). "Incentivizing water conservation in agriculture: a case study of the Great Salt Lake watersheds". In: *Environmental Research Letters* 20.1, p. 014063. DOI: 10.1088/1748-9326/ad99e8.

Liang, Yong et al. (2022). "Investigation of the influence of mineral dust on airborne particulate matter". In: *Atmospheric Environment*.

Los Angeles Department of Water and Power (2025). *Owens Lake Dust Mitigation Program: Budget and Expenditures Report*. Annual operating and maintenance costs for Owens Lake dust mitigation and cumulative expenditures. Los Angeles Department of Water and Power. URL: https://www.ladwp.com/who-we-are/ladwp-eastern-sierra/owens-lake.

PRISM Group (2014). Oregon State University. URL: https://prism.oregonstate.edu.

Querol, Xavier et al. (2019). "Monitoring the impact of desert dust outbreaks for air quality for health studies". In: *Environment International*.

Schlenker, Wolfram and W. Reed Walker (2016). "Airports, air pollution, and contemporaneous health". In: *The Review of Economic Studies* 83.2, pp. 768–809.

Tarboton, David and Madeline Merck (2023). *Great Salt Lake Bathymetry*.

U.S. Environmental Protection Agency (1997). *Owens Valley Particulate Matter Plan: Fact Sheet*. Archived EPA Region 9 Fact Sheet. Air monitoring of the Owens Valley during the past 18 years has measured the highest particulate matter ("PM-10") pollution in the United States. U.S. Environmental Protection Agency, Pacific Southwest Region. URL: https://19january2017snapshot.epa.gov/www3/region9/air/owens/fact.html.

U.S. Environmental Protection Agency (2016). *Treatment of Data Influenced by Exceptional Events*. Tech. rep. EPA.

— (2020). *Exceptional Events Rule: Guidance*. Tech. rep. EPA.

Utah Department of Environmental Quality (2025). *Inversions*. URL: https://deq.utah.gov/air-quality/inversions.

van Donkelaar, Aaron et al. (2024). "North American fine particulate matter chemical composition for 2000–2022 from satellites, models, and monitors: the changing contribution of wildfires". In: *ACS ES&T Air* 1.12, pp. 1589–1600.

Weller, Kristine (Oct. 28, 2022). "What's a Utah inversion and why is the air so icky?" In: *KUER 90.1*. URL: https://www.kuer.org/health-science-environment/2022-10-28/whats-a-utah-inversion-and-why-is-the-air-so-icky.

Williams, Emily (2021). "Reimagining exceptional events: Regulating wildfires through the Clean Air Act". In: *Wash. L. Rev.* 96, p. 765.

Wurtsbaugh, Wayne A. et al. (2017). "Decline of the Great Salt Lake". In: *Water*.

8 Appendix

A Supplemental Tables

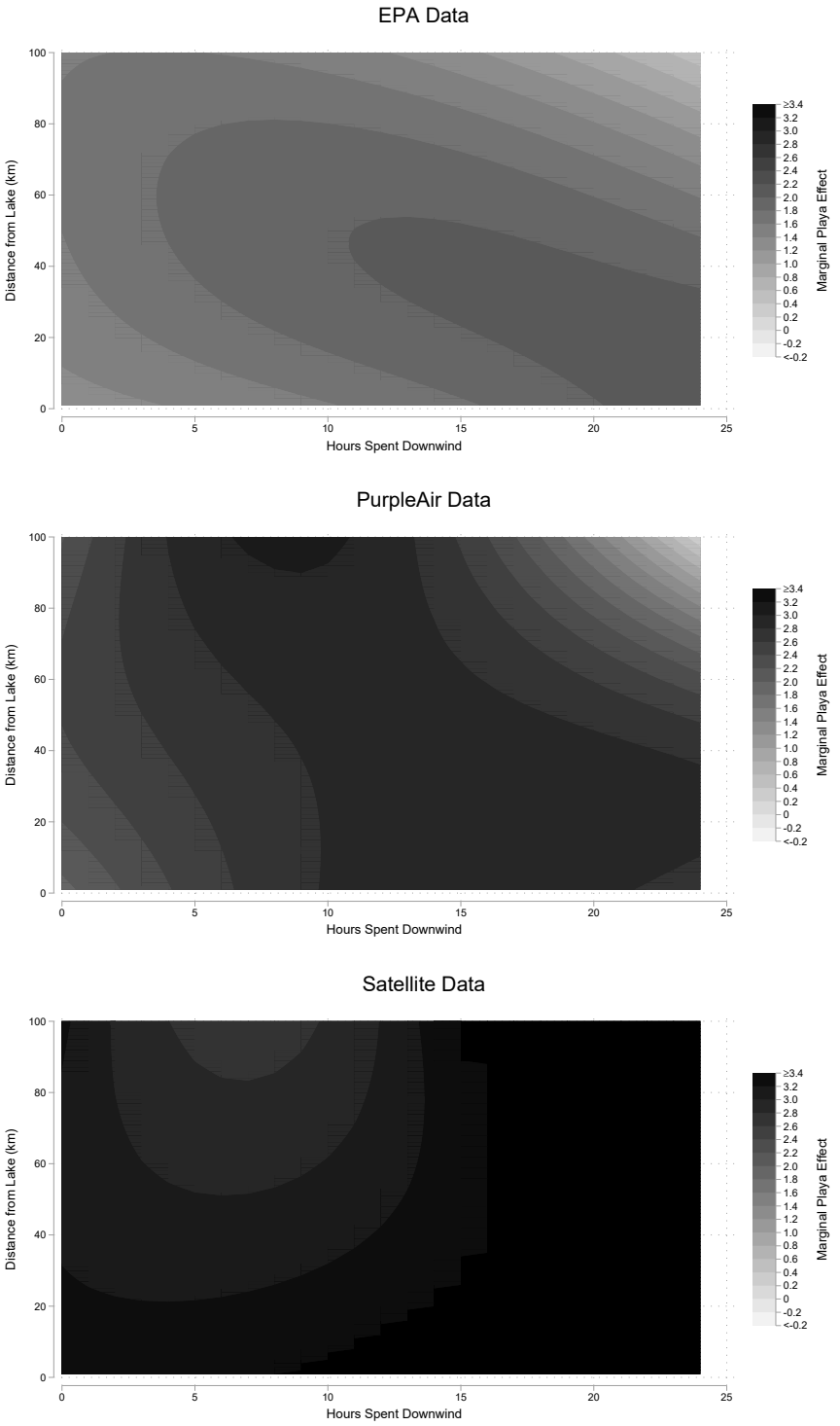
Table A1: HYSPLIT Marginal Effect Estimates

	(1) EPA Data	(2) PurpleAir Data	(3) Satellite Data
Dependent Variable: $PM_{2.5}$			
Particle Share × ln(Total Particles)	1.044	5.985***	40.844***
	(2.299)	(1.023)	(5.565)
R-squared	0.815	0.809	0.582
Observations	66,930	400,186	505,596
Dependent Variable: ln(Total Particles)			
Playa Area	0.124***	0.124***	0.121***
	(0.004)	(0.004)	(0.009)
R-squared	0.285	0.285	0.443
Observations	2,557	2,557	182
Mean Particle Share	0.016	0.016	0.018

Notes: Table presents estimates of the marginal effect of total particles on $PM_{2.5}$ concentrations, β from Eq. 8, in the top panel. Clustered standard errors are shown in parentheses. The second panel shows the coefficient estimate from a regression of total particles on playa area. Heteroskedastic robust standard errors are shown in parentheses.

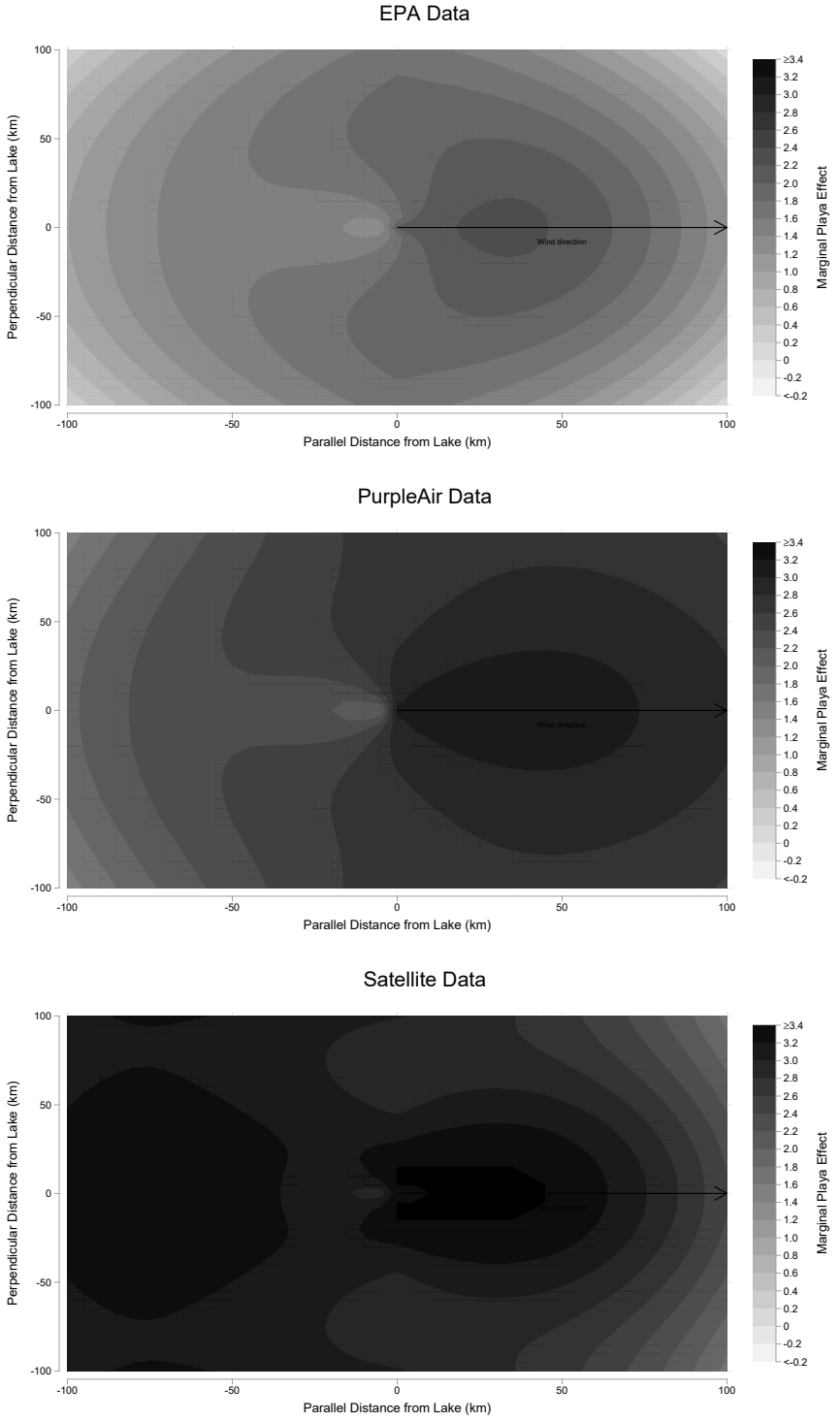
B Supplemental Figures

Figure A1: Hours Downwind Marginal Effect Estimates With Less Interactions



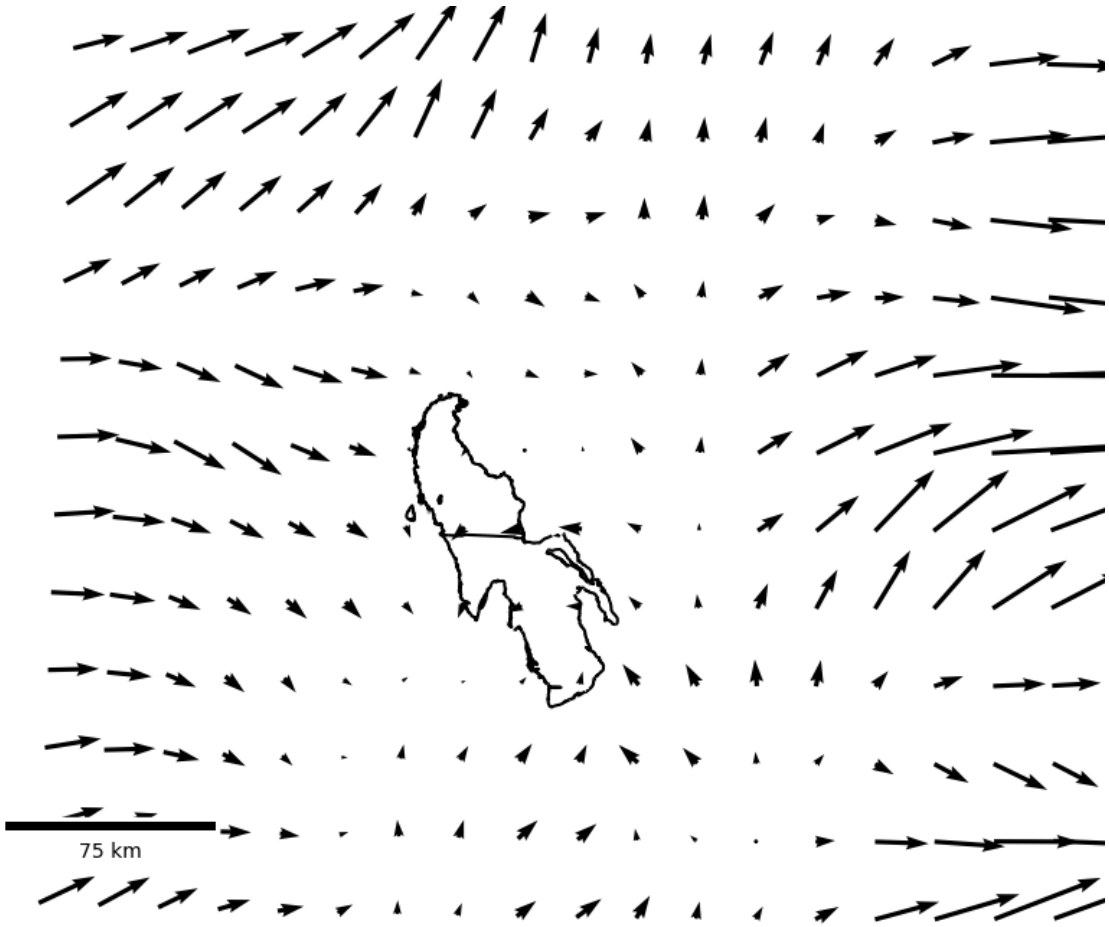
Notes: Figure plots the marginal effect estimate gradient over distance from the lake and the number of hours spent downwind. Marginal effect is estimated from Eq. 4 without the interactions with wind speed and only using non-winter observations. Marginal playa effect is interpreted as the $\mu g/\text{m}^3$ increase in $\text{PM}_{2.5}$ arising from a 100 km^2 increase in playa area.

Figure A2: Angle Downwind Marginal Effect Estimates With Less Interactions



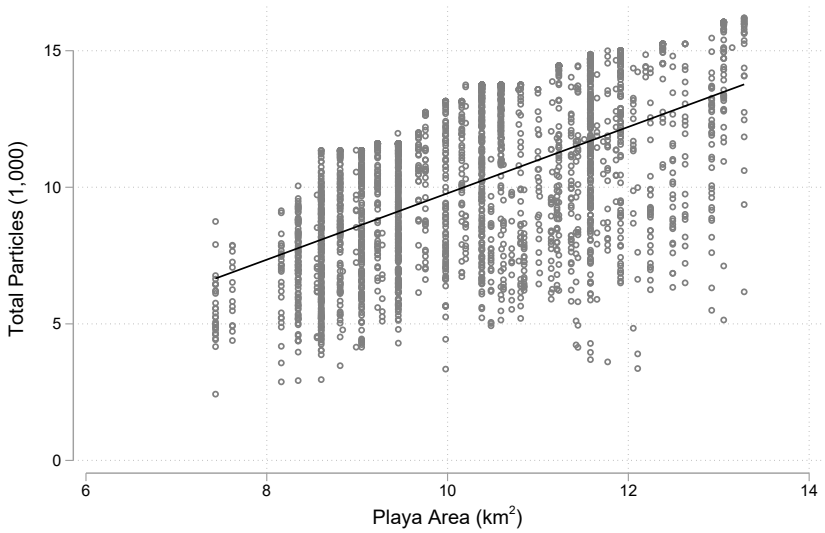
Notes: Figure plots the marginal effect estimate gradient over location relative to the lake. Marginal effect is estimated from Eq. 6 without the interactions with wind speed and only using non-winter observations. Distance north is shown on the y-axis, and distance east on the x-axis. The lake is located at the point (0,0). Marginal playa effect is interpreted as the $\mu g/\text{m}^3$ increase in $\text{PM}_{2.5}$ arising from a 100 km^2 increase in playa area.

Figure A3: Average Wind Vectors



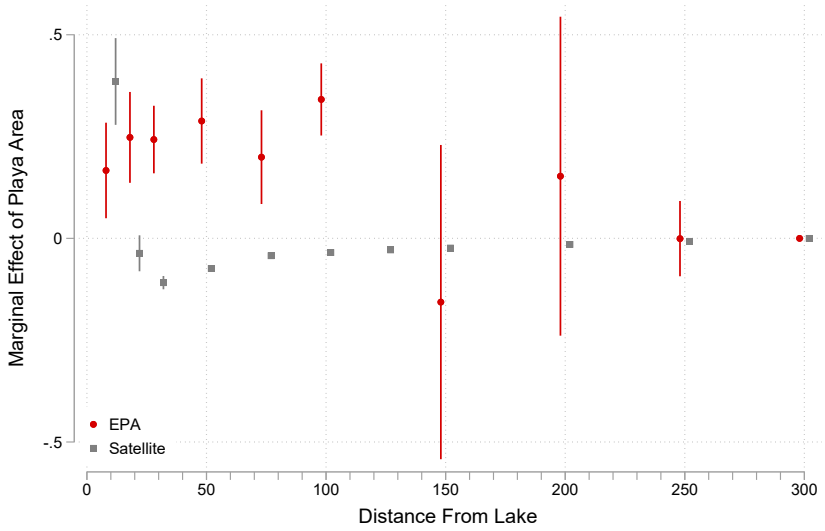
Notes: Figure plots the average wind vectors over the sample time frame. The arrow head indicates in which direction wind is blowing on average, while arrow length indicates average wind speed, with longer arrows reflecting higher speed.

Figure A4: Playa Area and Total Particles Correlation



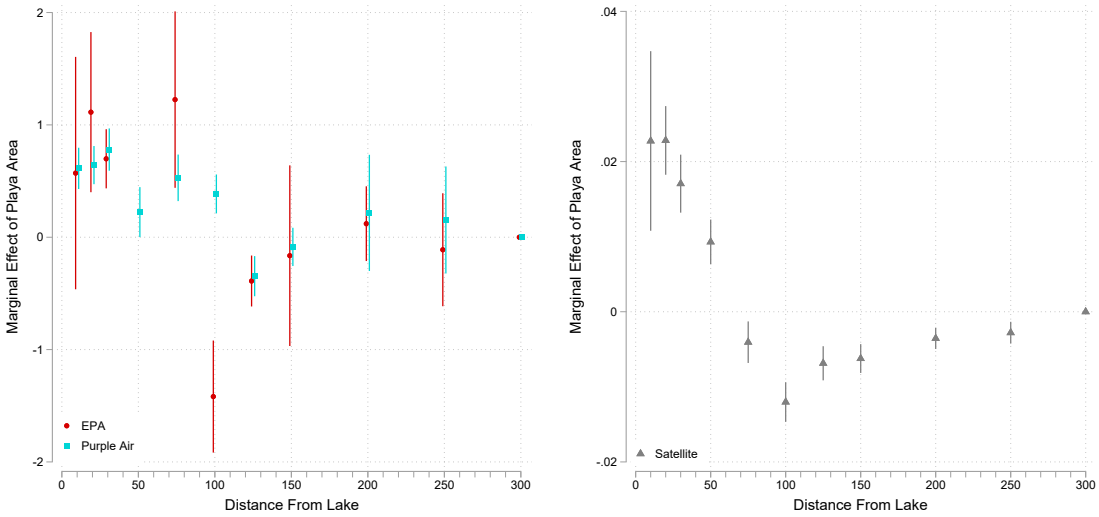
Notes: Figure plots sample observations of playa area and total modeled particle emissions.

Figure A5: Near-Far Marginal Effect Estimates for All Years



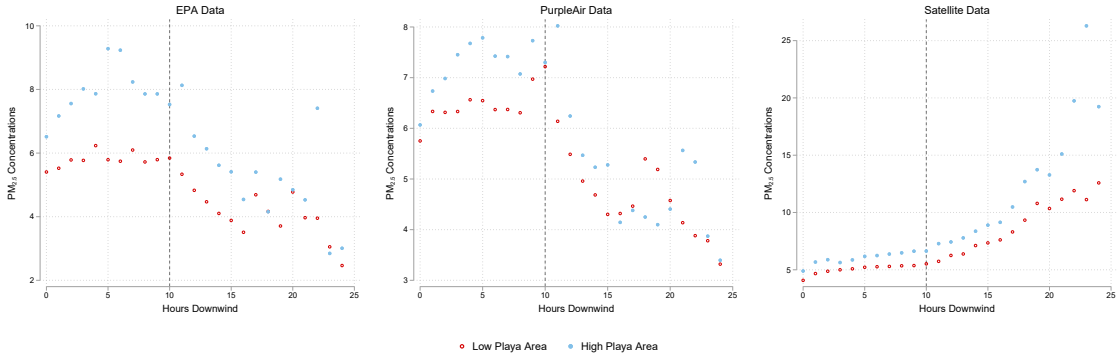
Notes: Figure plots the marginal effect estimate gradient from Eq. 2 over distance from the lake. The sample used for analysis contains all observations occurring since 2000. Marginal playa effect is interpreted as the $\mu g/\text{m}^3$ increase in $\text{PM}_{2.5}$ arising from a 100 km^2 increase in playa area, relative to the effect at 300 km from the lake. 95% confidence intervals for standard errors clustered at the point level are shown as vertical lines.

Figure A6: Near-Far Marginal Effect Estimates for PM_{10}



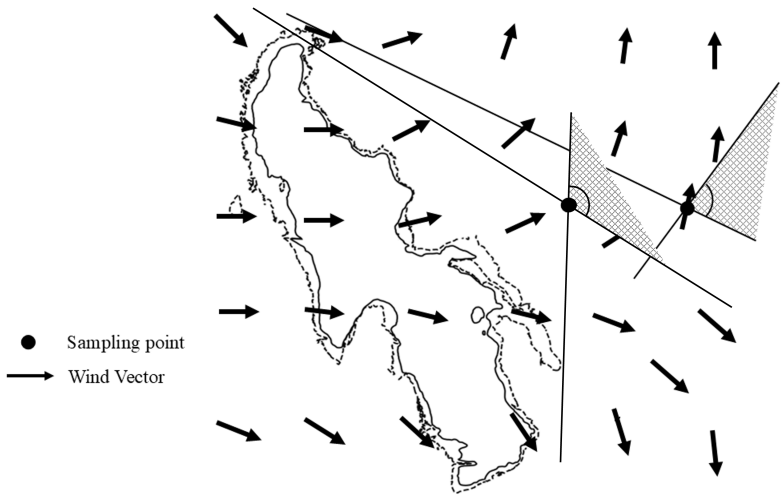
Notes: Figure plots the marginal effect estimate gradient from Eq. 2 using PM_{10} or dust as the outcome variable of interest. Left figure shows results for PM_{10} measured by EPA and PurpleAir monitors. Right figure shows results for dust measured by satellite. Marginal playa effect is interpreted as the $\mu g/m^3$ increase in PM_{10} or dust arising from a 100 km^2 increase in playa area, relative to the effect at 300 km from the lake. 95% confidence intervals for standard errors clustered at the point level are shown as vertical lines.

Figure A7: Correlation Between $PM_{2.5}$ Concentrations and Hours Spent Downwind



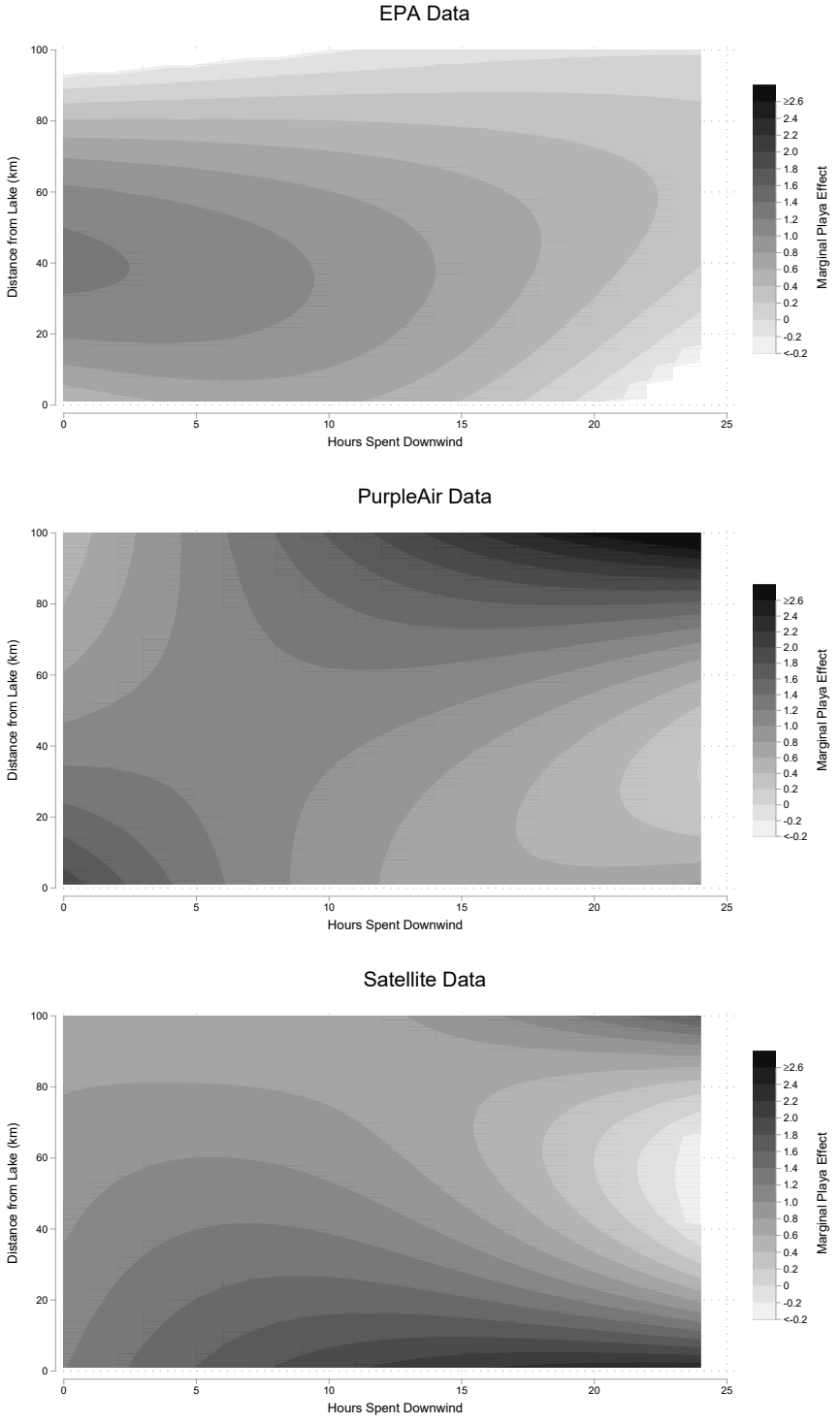
Notes: Figure plots average $PM_{2.5}$ concentration as a function of hours spent downwind for the main analysis samples. Averages are conditional on tercile of playa area, with low playa area being the bottom tercile and high playa area being the top.

Figure A8: Downwind Angle Set Over Space



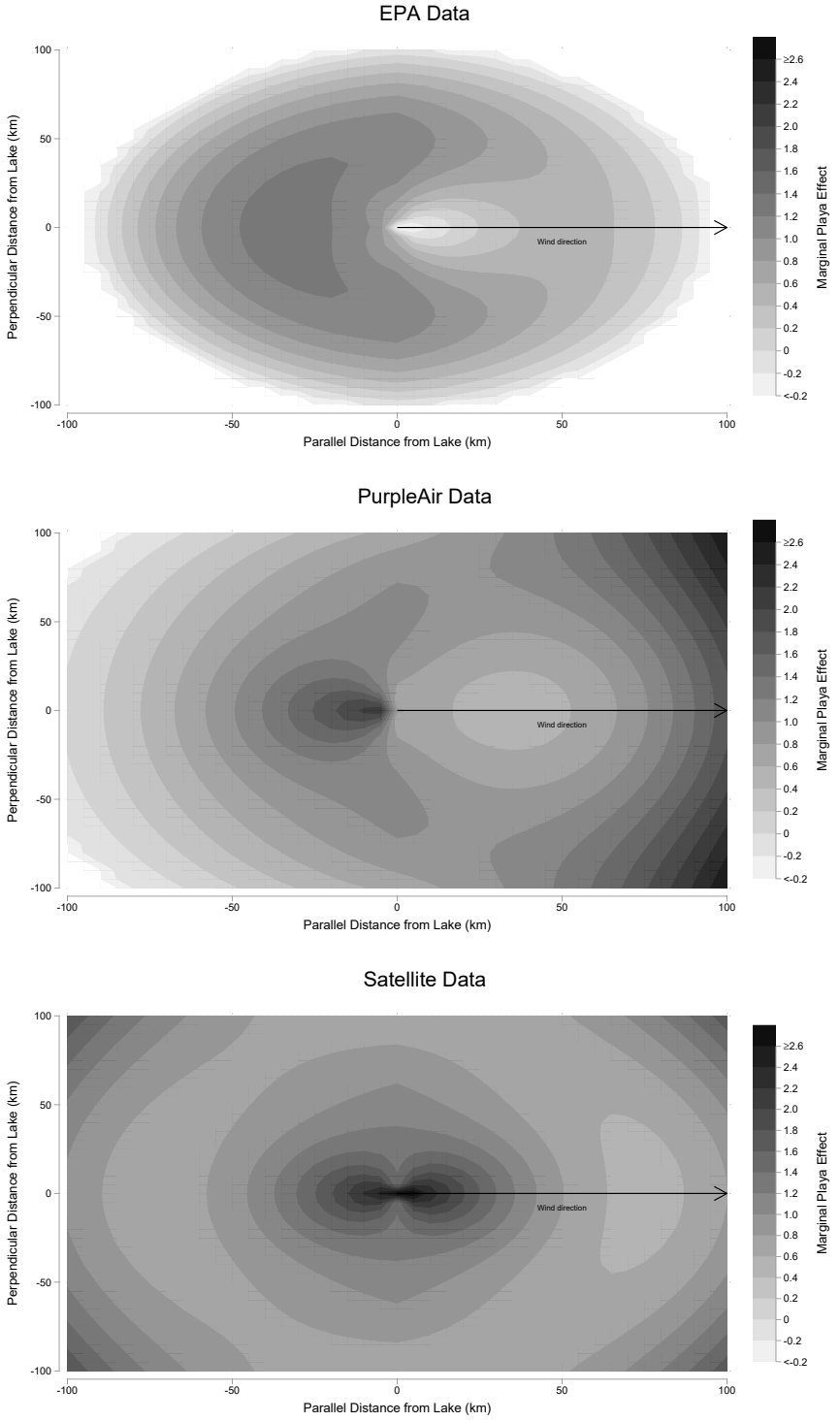
Notes: Figure diagrammatically represents the decrease in the magnitude of the set of downwind angles, $\mathcal{A}_p$ shown as the shaded gray area, as distance from the lake increases. Wind vectors over space are denoted by the black arrows and example sampling points as solid dots.

Figure A9: Hours Downwind Marginal Effect Estimates in Winter



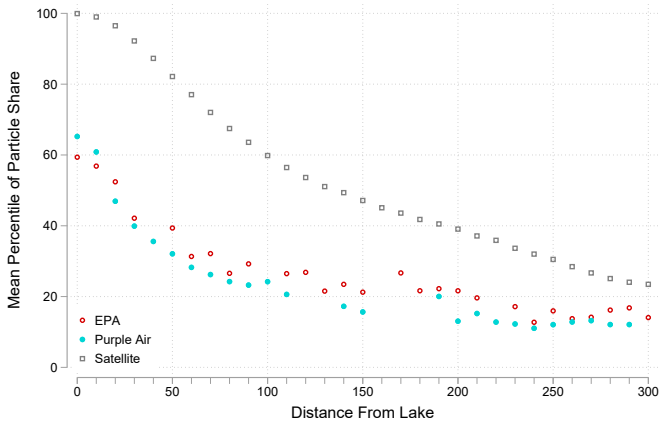
Notes: Figure plots the marginal effect estimate gradient from Eq. 4 over distance from the lake and the number of hours spent downwind. Marginal playa effect is interpreted as the $\mu g/\mathrm{m}^3$ increase in $\mathrm{PM}_{2.5}$ arising from a 100 km^2 increase in playa area. The calculation assumes a winter period and a wind speed of 1.67.

Figure A10: Angle Downwind Marginal Effect Estimates in Winter



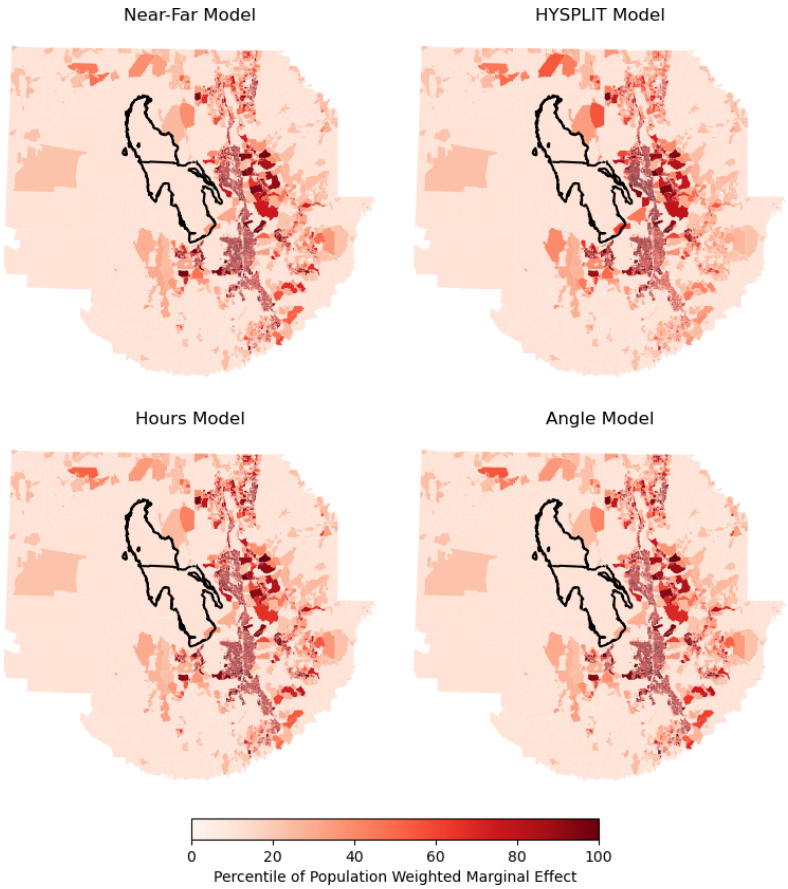
Notes: Figure plots the marginal effect estimate gradient from Eq. 6 over location relative to the lake. Distance north is shown on the y-axis, and distance east on the x-axis. The lake is located at the point (0,0). Marginal playa effect is interpreted as the $\mu g/\mathrm{m}^3$ increase in $\mathrm{PM}_{2.5}$ arising from a 100 km^2 increase in playa area. The calculation assumes a winter period, a wind direction of going due-east, and a wind speed of 1.67.

Figure A11: Particle Shares Over Space



Notes: Figure plots the average decile of particle shares for sample points based on distance from the lake.

Figure A12: Population Weighted Marginal Effect Estimate Maps



Notes: Figure plots the percentile of the average of the marginal increase in $PM_{2.5}$ concentration scaled by block population. Estimates are for 2023. The percentile for a given block is calculated relative to all other blocks under the given model.